Supporting Information

Fixation of atmospheric CO_2 as C1-feedstock by nickel(II) complexes

Sethuraman Muthuramalingam[a], Marappan Velusamy[b], and Ramasamy Mayilmurugan*[,a]

[a]Bioinorganic Chemistry Laboratory/Physical Chemistry, School of Chemistry, Madurai Kamaraj University, Madurai 625021, India. Email: mayilmurugan.chem@mkuniversity.ac.in

[b]Department of Chemistry, North Eastern Hill University, Shillong 793022, India.

Table of Contents

Materials: Commercially available chemicals were used without further purification. 1-methylhomopiperazine, $Ni(ClO_4)_2 \cdot 6H_2O$, 2-quinolylchloride hydrochloride, 2-vinyl pyridine, 2-picolylchloride hydrochloride, 2-chloromethyl-4-methoxy-3,5-dimethylpyridine hydrochloride, $NaBPh_4$, tetrabutylammonium perchlorate (TBAP), triethylamine, and chloroform-*d* were purchased from Aldrich chemicals. Sodium hydroxide, sodium hydrogen carbonate, sodium sulfate anhydrous, lithium perchlorate, acetic acid, silica gel, acetonitrile, chloroform, hexane, and toluene were purchased from Merck, India and used after appropriate distillation or purification.

Instrumentation. The NMR spectra were recorded on a 300 MHz Bruker. ESI-Mass spectra recorded using a Thermo LC-MS instrument. UV-vis spectra and kinetic data obtained using the Agilent diode array spectrometer (Agilent 8453). Elemental analyses carried out using a Heraeus Vario Elemental automatic analyzer. Cyclic Voltammetry (CV) performed using a three-electrode cell configuration (CHI, model 440). A platinum sphere (acetonitrile medium), platinum wire, and $Ag(s)/Ag^+$ were used as working, auxiliary, and reference electrodes respectively. The Bu_4NClO_4 were used as supporting electrolyte in acetonitrile. The $E_{1/2}$ values were observed under identical conditions. GC-MS and GC analysis performed on Agilent 5977E GCMSD using HP-5 MS ultra-inert (30 m × 250 μm × 0.25 μm) capillary column.

X-ray Crystal Structure Analysis. Single crystal X-ray diffraction measurements were performed on the Agilent Technologies Supernova-E CCD diffractometer. The suitable single crystal of **1, 1a, 2a,** and **4a** with suitable size were selected from the mother liquor and immersed in paraffin oil, then mounted on the tip of glass fibre. The structures were solved by direct methods using the program SHELXS-2013. Refinement and all further calculations were carried out using SHELXL-2013. The H-atoms were included in calculated positions and treated as riding atoms using the SHELXL default parameters. The non-H atoms were refined anisotropically, using weighted full-matrix least-squares on F^2. CCDC 1975592, 1975593, 1975594, and 1975598 are containing the supplementary crystallographic data for this paper. These data can be obtained free of charge from The Cambridge Crystallographic Data Centre via ww.ccdc.cam.ac.uk/data request/cif.

NMR data for Cyclic carbonates:

4-Methyl-1,3-dioxolan-2-one: ^{1}H NMR (300 MHz, $CDCl_3$): δ = 4.75-4.82 (m, 1H), 4.45-4.51 (m, 1H), 3.91-3.97 (m, 1H), 1.36 (d, *J* = 1.37 Hz, 3H) ppm. ^{13}C NMR (300 MHz, $CDCl_3$): δ, 155.52, 74.08, 71.09, 19.60 ppm. GC-MS (*m/z*): 102.01.

4-Phenyl-1,3-dioxolan-2-one: ^{1}H NMR (300 MHz, $CDCl_3$): δ = 7.21-7.40 (m, 5H), 5.66-5.71 (t, *J* = 5.69 Hz, 1H), 4.78-4.83 (t, *J* = 4.81 Hz, 1H), 4.26-4.32 (t, *J* = 4.29 Hz, 1H) ppm. ^{13}C NMR (300 MHz, $CDCl_3$): δ = 155.38, 136.23, 130.06, 129.57, 126.30, 78.43, 71.67 ppm. GC-MS (*m/z*): 164.10.

1,3-benzodioxolan-2-one: ^{1}H NMR (300 MHz, $CDCl_3$): δ = 4.64 (m, 2H), 1.73 (m, 2H), 1.48 (m, 4H), 1.34 (m, 2H) ppm. ^{13}C NMR (300 MHz, $CDCl_3$): δ = 155.82, 76.21, 27.06, 24.45 ppm. GC-MS (*m/z*): 142.20.

4-(chloromethyl)-1,3-dioxolan-2-one: ^{1}H NMR (300 MHz, $CDCl_3$): δ = 5.01 (m, 1H), 4.57-4.62 (t, *J* = 4.60 Hz, 1H), 4.43 (dd, *J* = 4.42 Hz, 1H), 3.79 (m, 2H). ^{13}C NMR (300 MHz, $CDCl_3$): δ = 154.66, 74.78, 67.38, 44.20 ppm. GC-MS (*m/z*): 135.90.

4-Butyl 1,3-dioxolan-2-one: ^{1}H NMR (300 MHz, $CDCl_3$): δ = 4.60-4.80 (m, 1H), 4.46-4.49 (t, *J* = 4.47 Hz, 1H), 3.98 (m, 1H), 1.22-1.33 (m, 6H), 0.84 (t, *J* = 0.84 Hz, 3H) ppm. ^{13}C NMR (300 MHz, $CDCl_3$): δ = 155.48, 77.25, 69.84, 33.77, 26.68, 22.48, 14.01 ppm. GC-MS (*m/z*): 144.20.

4-ethyl-1,3-dioxolan-2-one: ^{1}H NMR (300 MHz, $CDCl_3$): δ = 4.48 (m, 1H), 4.30 (m, 1H), 4.01 (m, 1H), 1.34 (m, 2H), 0.92 (t, 3H). ^{13}C NMR (300 MHz, $CDCl_3$): δ = 155.91, 78.51, 69.52, 24.35, 13.92 ppm. GC-MS (*m/z*): 116.10.

4,4-dimethyl-1,3-dioxolan-2-one: ^{1}H NMR (300 MHz, $CDCl_3$): δ = 4.06 (m, 2H), 1.46 (s, 6H). ^{13}C NMR (300 MHz, $CDCl_3$): δ = 154.16, 87.68, 75.41, 27.63 ppm. GC-MS (*m/z*): 116.00.

4-(allyloxymethyl)-1,3-dioxolan-2-one: ^{1}H NMR (300 MHz, $CDCl_3$): 5.73 (m, 1H), 5.17 (m, 2H), 4.71 (m, 1H), 4.40 (m, 1H), 4.25 (m, 1H), 3.90 (m, 2H), 3.58 (m, 2H). ^{13}C NMR (300 MHz, $CDCl_3$): δ = 155.41, 133.96, 117.23, 77.67, 69.14, 66.55, 66.12 ppm. GC-MS (*m/z*): 158.00.

Kinetic Studies. The CO_2 fixation kinetics has been studied by time-dependent spectrophotometry measurements at 25 °C. The intermediates $[(LNi)_2(CO_3)]^{2+}$ were generated by treating the stoichiometric amount of complexes **1 - 4** (1×10^{-3} M) with CO_2 in the presence of Et_3N (2

equivalents) in acetonitrile. The formation constant of the intermediates $[(LNi)_2(CO_3)]^{2+}$ has been determined by monitoring the new absorbance bands around at 592 - 681 nm.

The intermediate $[(LNi)_2(CO_3)]^{2+}$ was freshly generated from **1 – 4** (1×10^{-3} M) with 2 equivalents of Et_3N in the presence of 1 bar CO_2 in acetonitrile. After reaching maximum intensity at 592 - 693 nm, the substrate epichlorohydrin has been added via microsyringe into the reaction mixture at 70 °C. Then, the reaction was carefully monitored by diode array spectrometer and the decay constants of the $[(LNi)_2(CO_3)]^{2+}$ were determined. After a while, the reaction mixture was passed through a silica column and the formation of cyclic carbonate was confirmed by GC-MS/GC and ^{1}H and ^{13}C NMR.

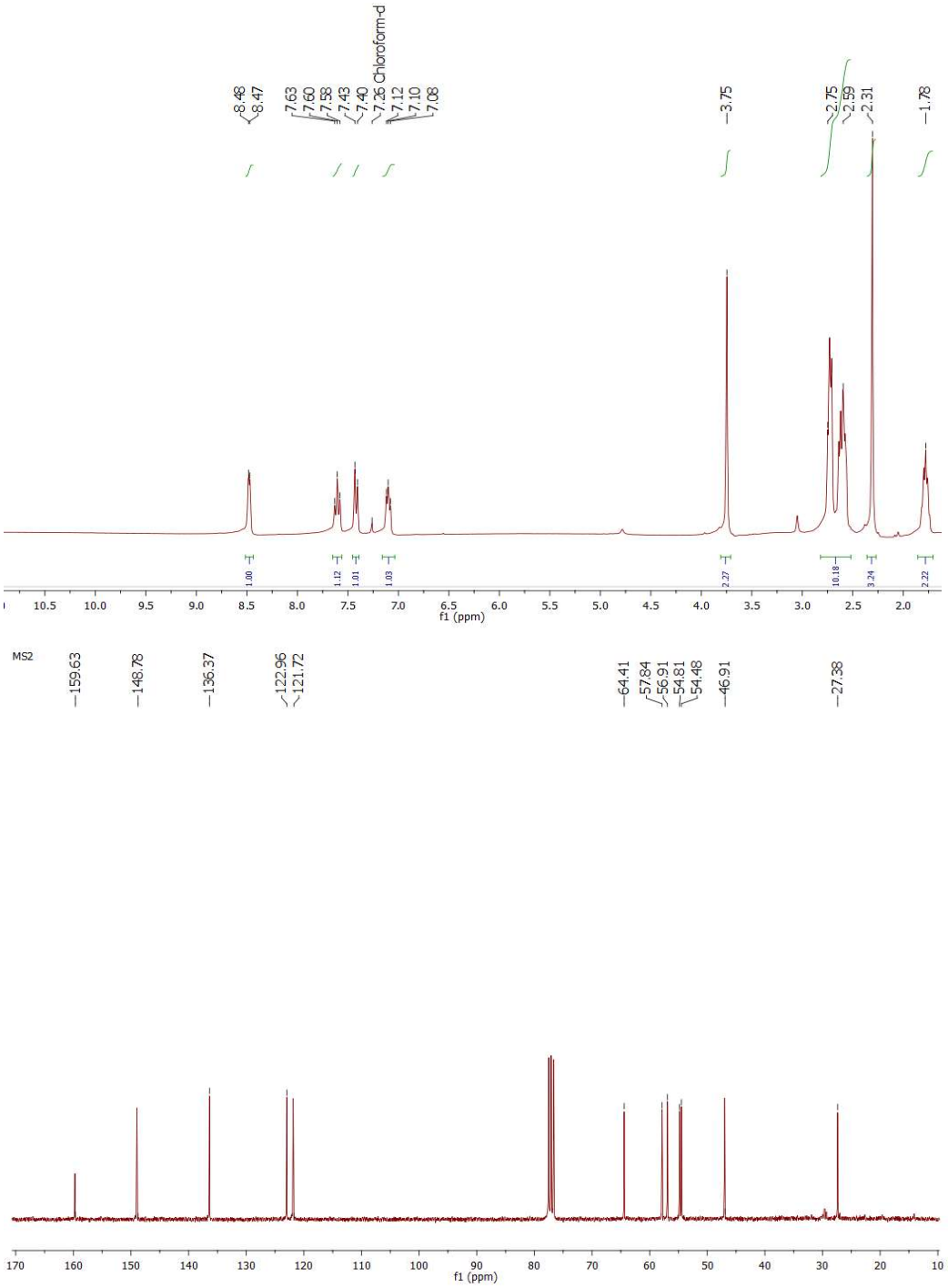

Figure S1. ^{1}H and ^{13}C NMR spectra for L1 in $CDCl_3$.

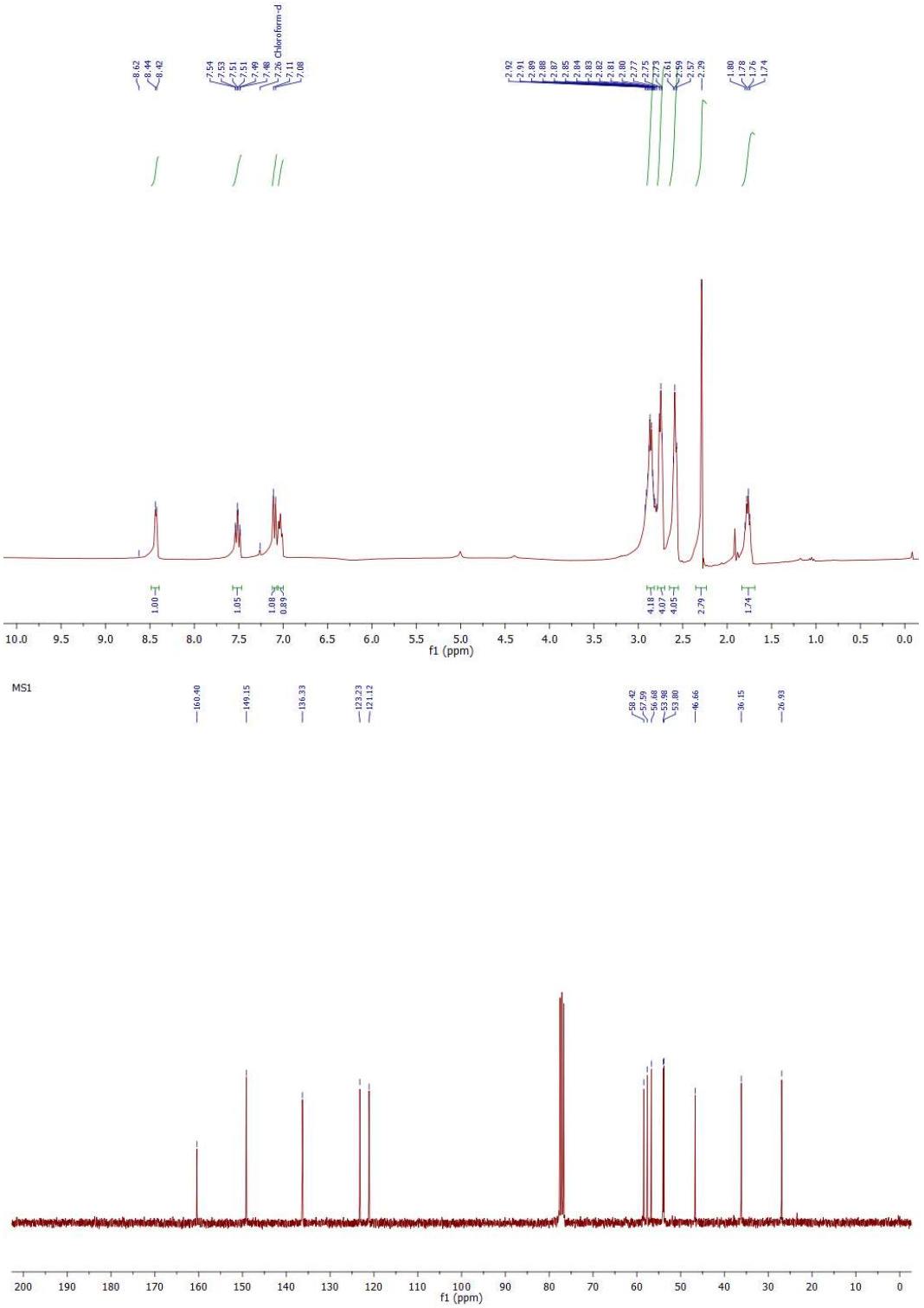

Figure S2. ^{1}H and ^{13}C NMR spectra for L2 in $CDCl_3$.

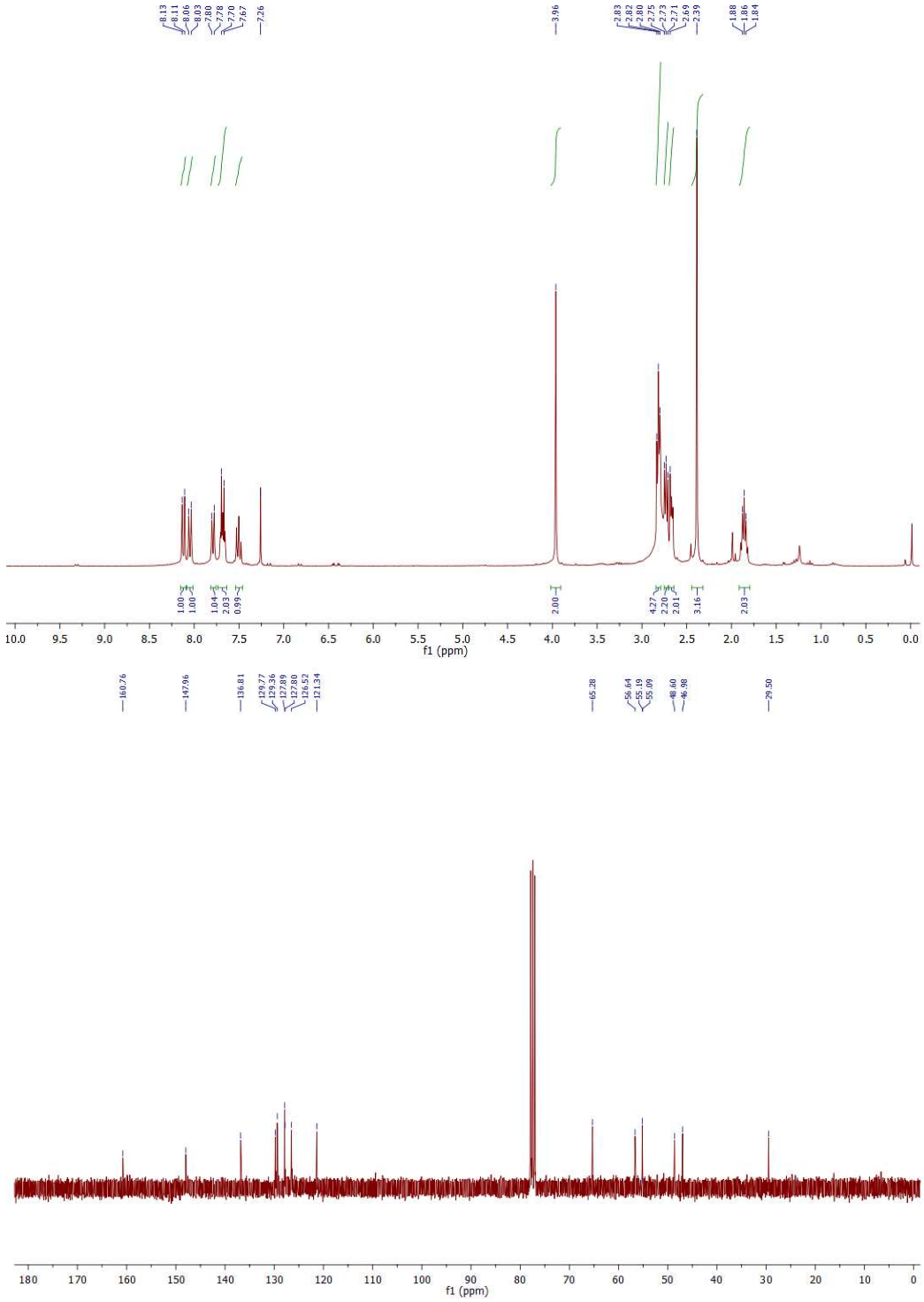

Figure S3. ^{1}H and ^{13}C NMR spectra for L3 in $CDCl_3$.

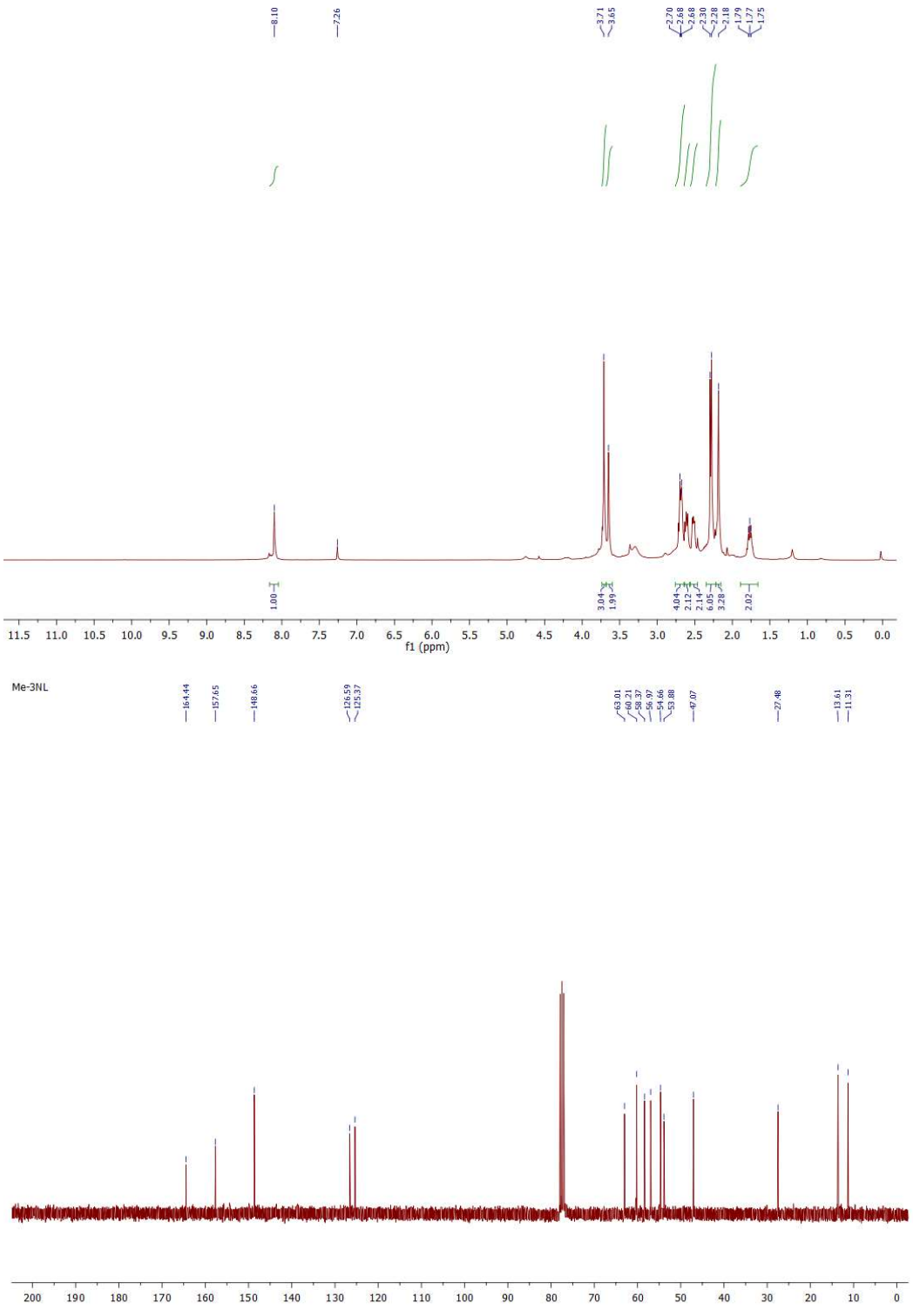

Figure S4. ^{1}H and ^{13}C NMR spectra for L4 in $CDCl_3$.

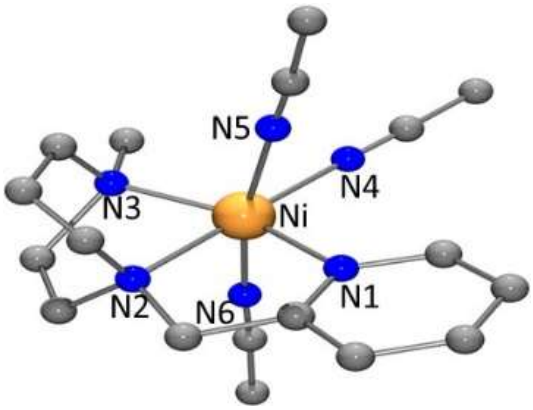

Figure S5. Molecular structure of $[Ni(L1)(CH_3CN)_3](BPh_4)_2$, **1**. The hydrogen atoms and BPh_4^- are omitted for clarity.

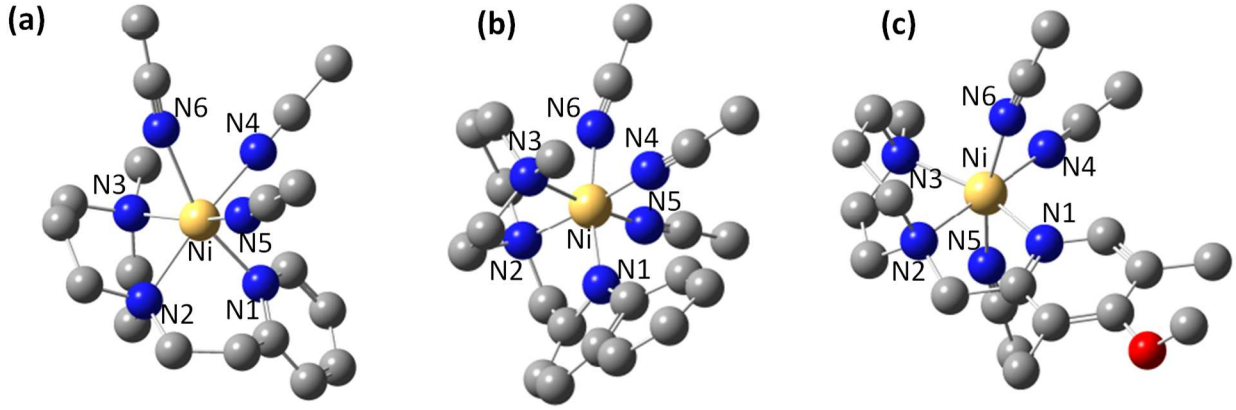

Figure S6. Optimized structure of **2** (a)**, 3** (b) and **4** (c) using B3LYP 631-G/ LANL2DZ basis set.

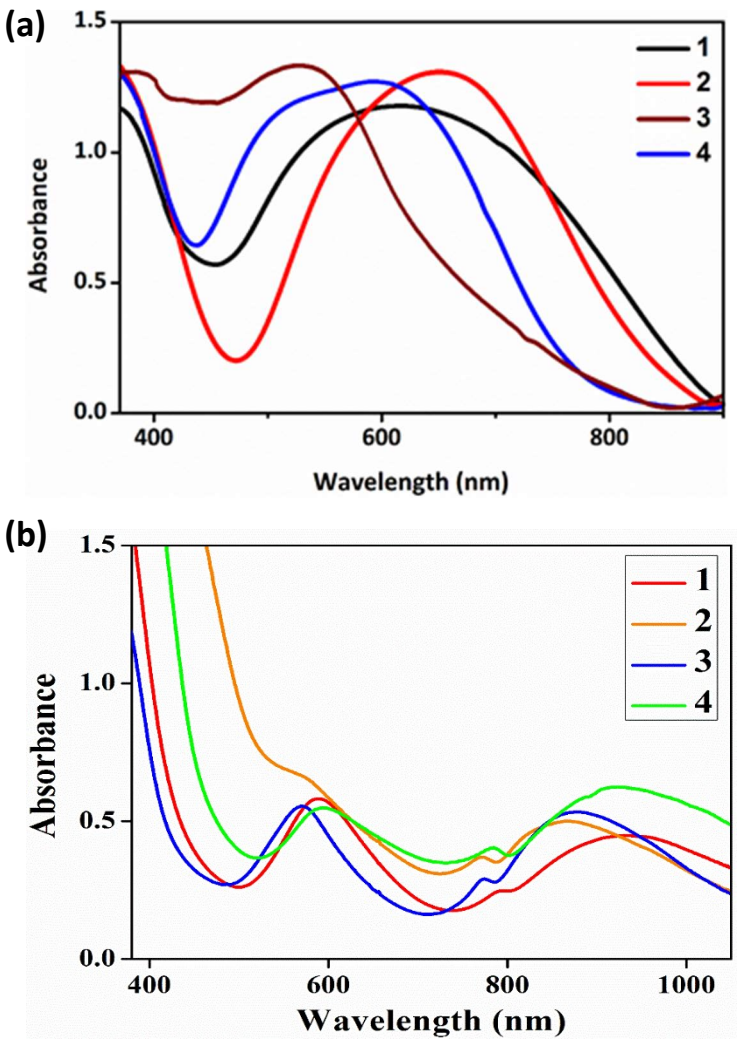

Figure S7. **(a)** Solid-state absorption spectra of **1 – 4**. **(b)** Electronic spectra of **1 – 4** (1×10^{-3} M) in acetonitrile at 25 ˚C.

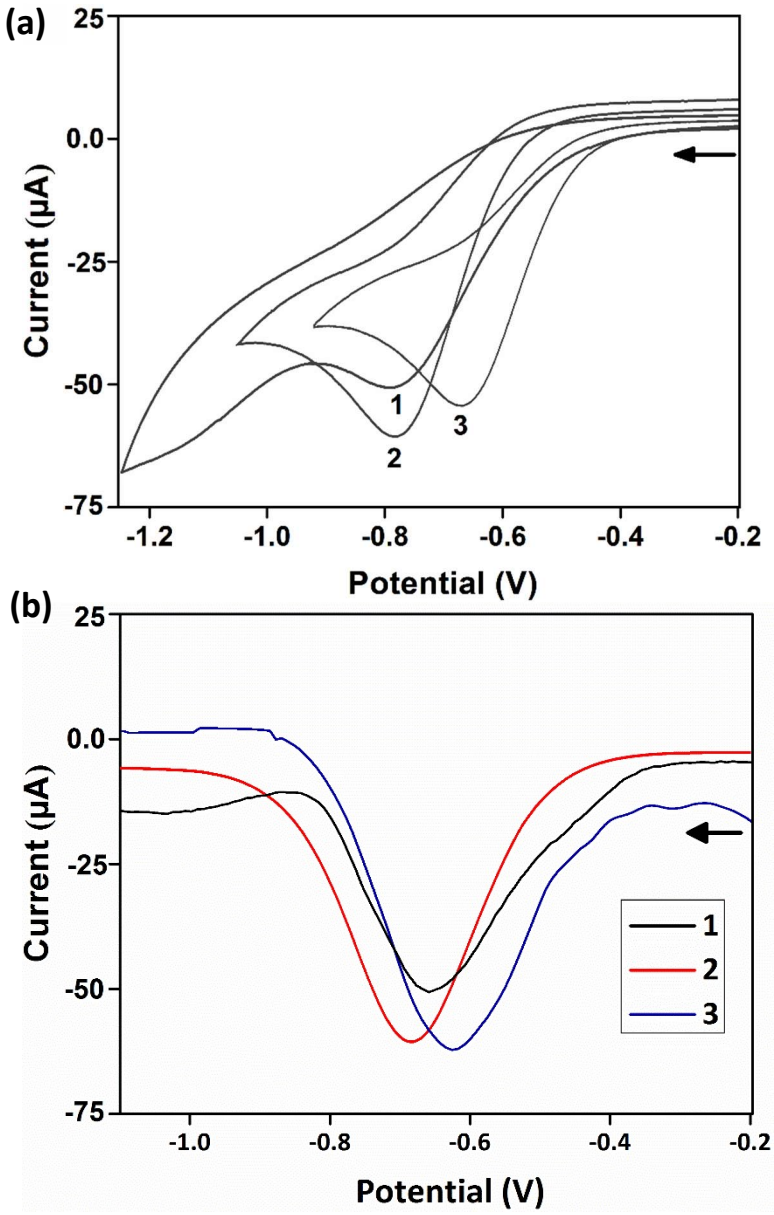

Figure S8. **(a)** Cyclic voltammograms and **(b)** DPV of **1 - 3** (1×10^{-3} M) in acetonitrile at 25 ˚C. Supporting electrolyte: TBAP (0.1 M); Reference electrode: Ag/Ag^{+} (non-aqueous); Working electrode: Pt-sphere. Scan rate = 100 mV s^{-1}.

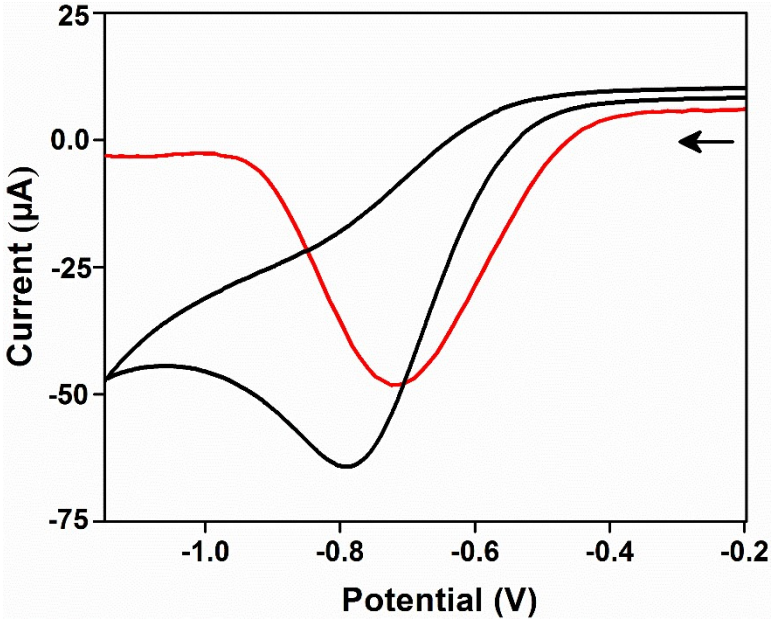

Figure S9. Cyclic voltammograms and DPV of **4** (1×10^{-3} M) in acetonitrile at 25 ˚C. Supporting electrolyte: TBAP (0.1 M); Reference electrode: Ag/Ag^{+} (non-aqueous); Working electrode: Pt-sphere. Scan rate = 100 mV s^{-1}.

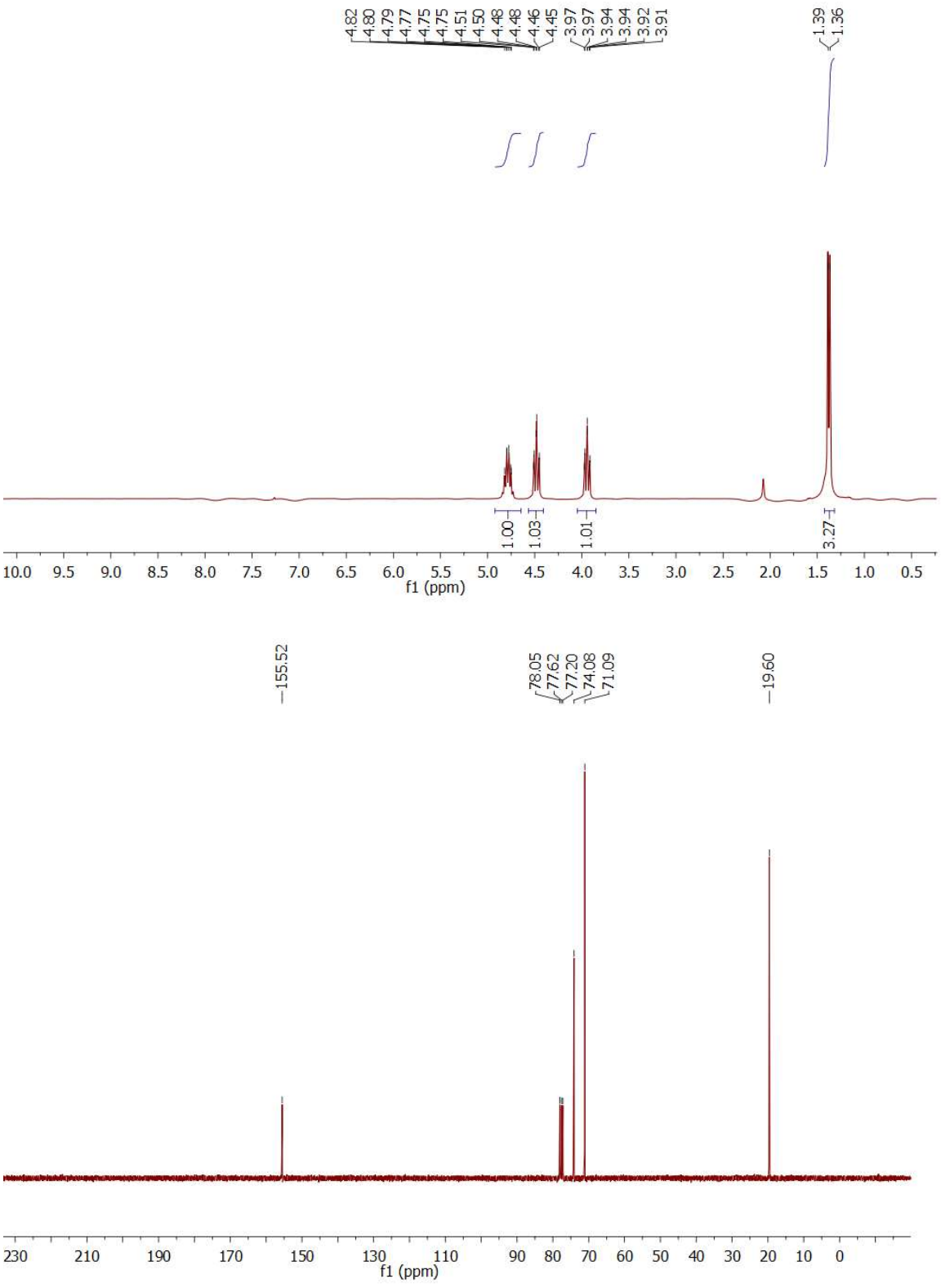

Figure S10. ^{1}H and ^{13}C NMR spectra of 4-methyl-1,3-dioxolan-2-one in $CDCl_3$.

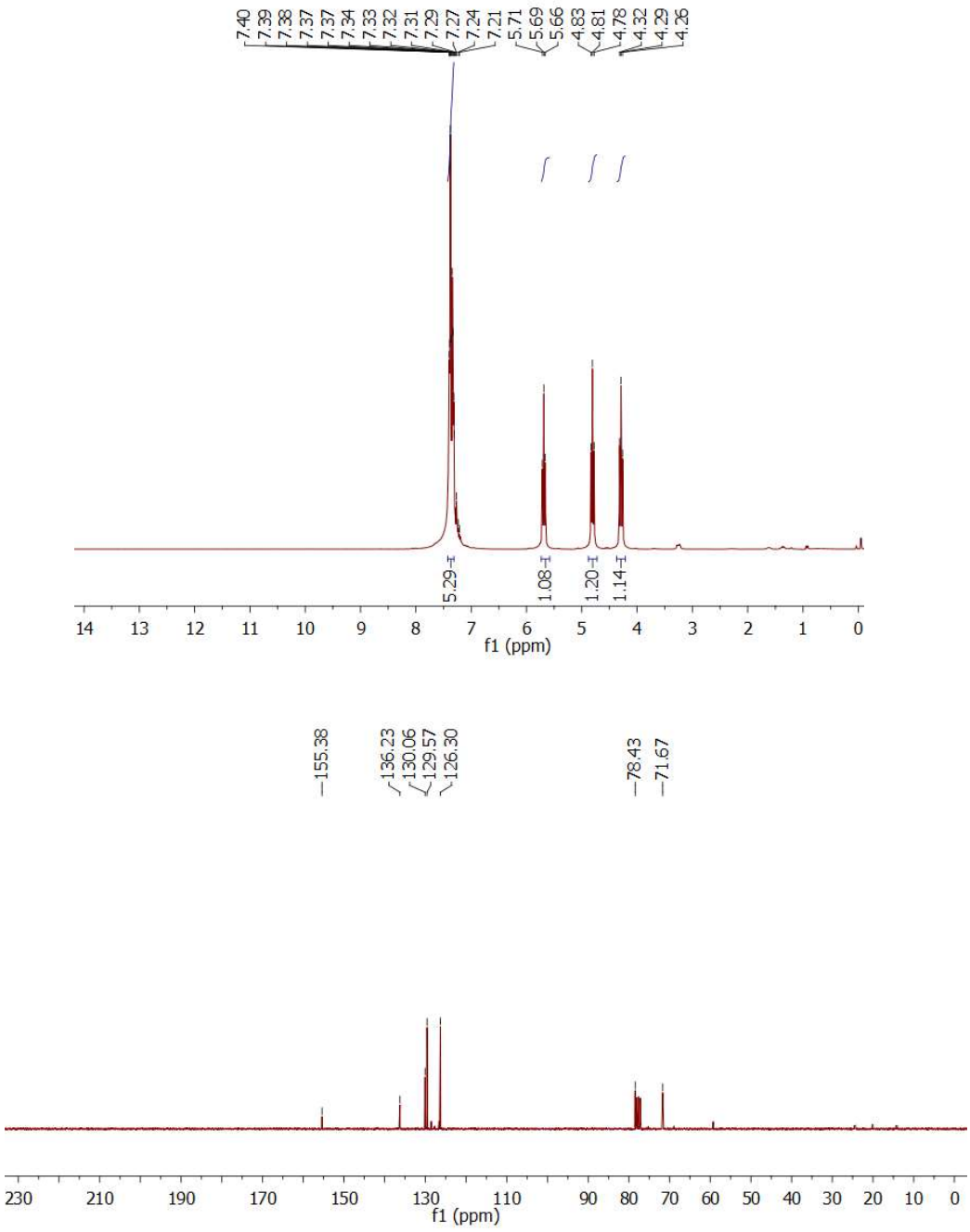

Figure S11. ^{1}H and ^{13}C NMR spectra of 4-phenyl-1,3-dioxolan-2-one in $CDCl_3$.

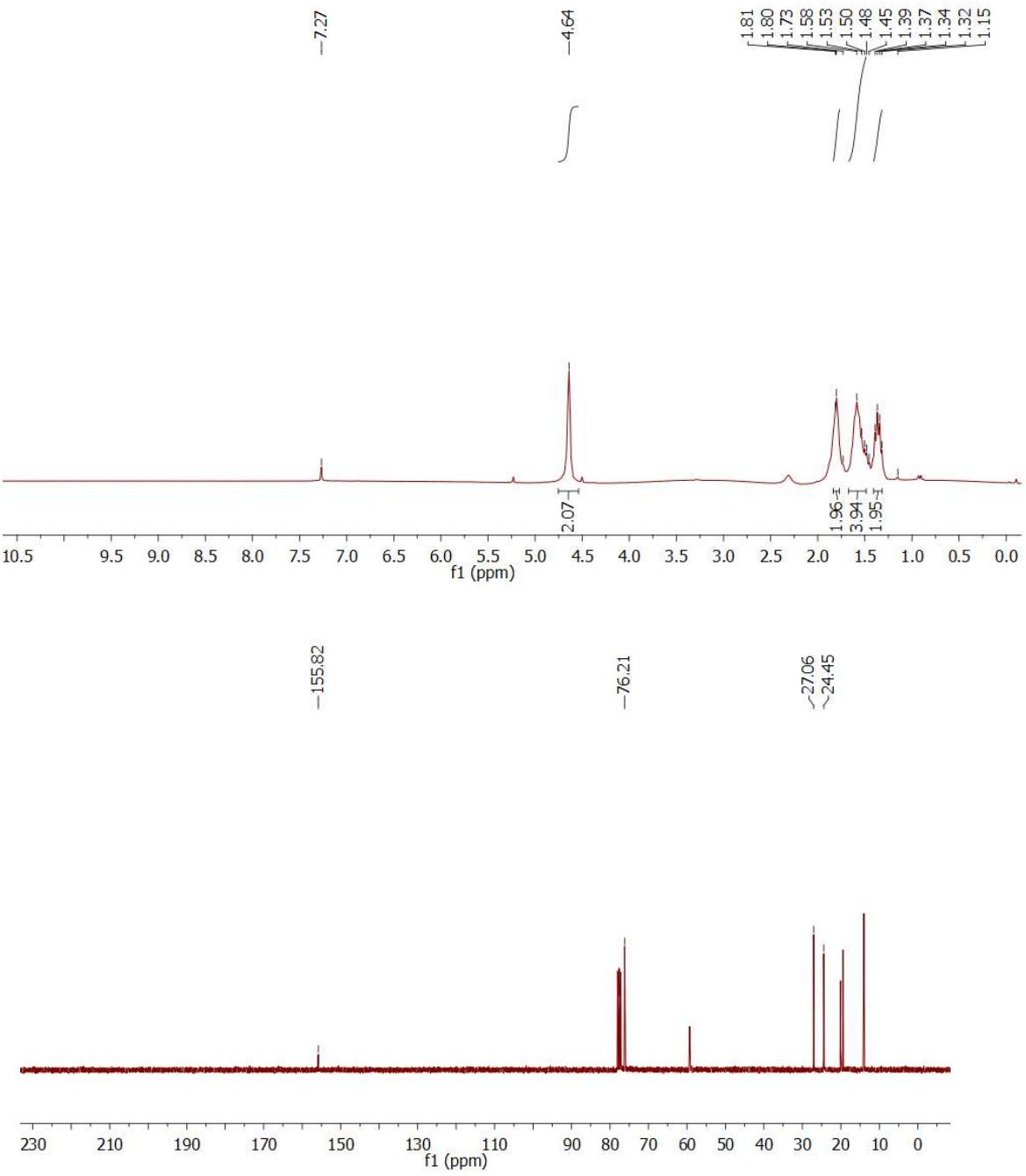

Figure S12. ^{1}H and ^{13}C NMR spectra of 1,3-benzodioxolan-2-one in $CDCl_3$.

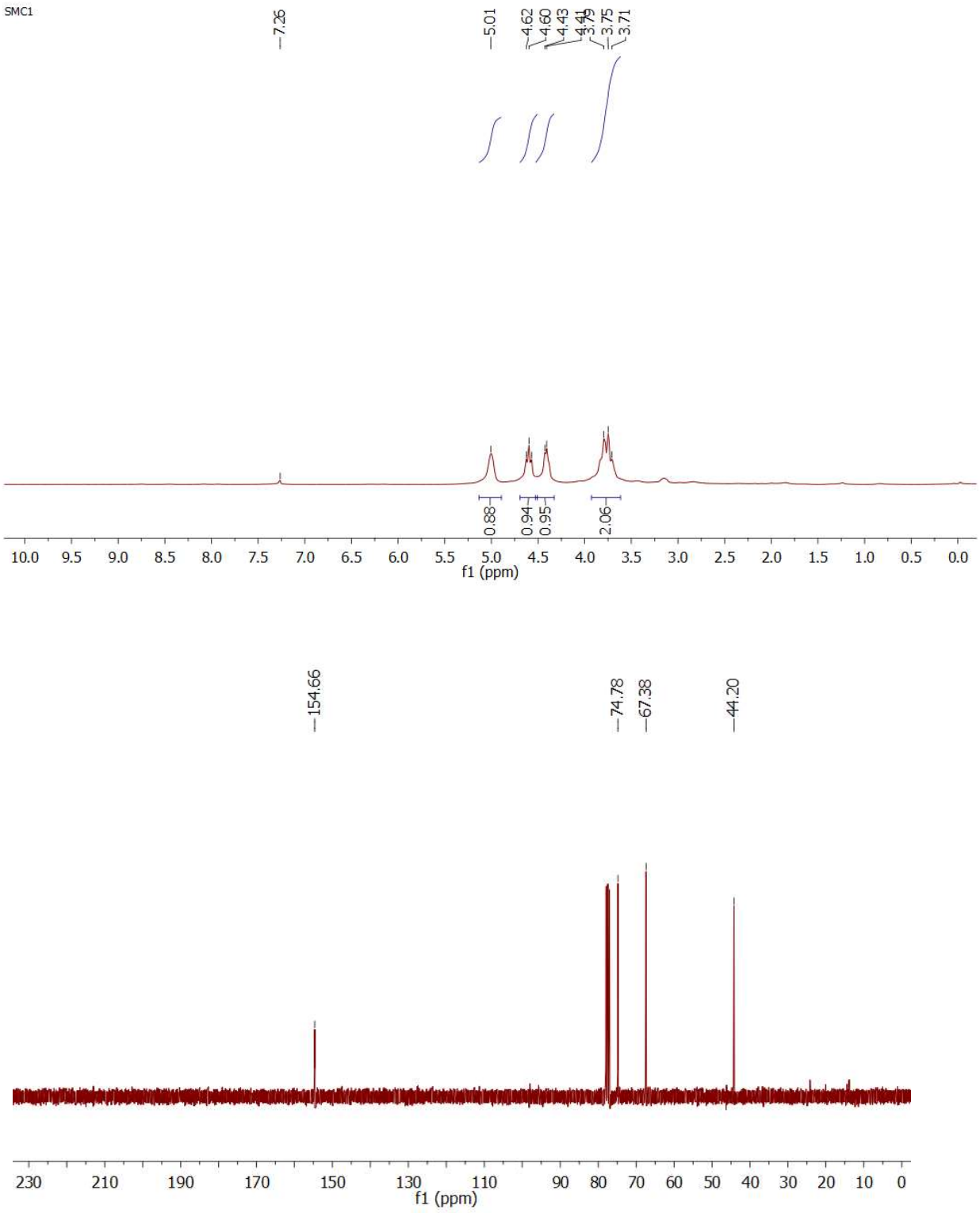

Figure S13. ^{1}H and ^{13}C NMR spectra of 4-(chloromethyl)-1,3-dioxolan-2-one in $CDCl_3$.

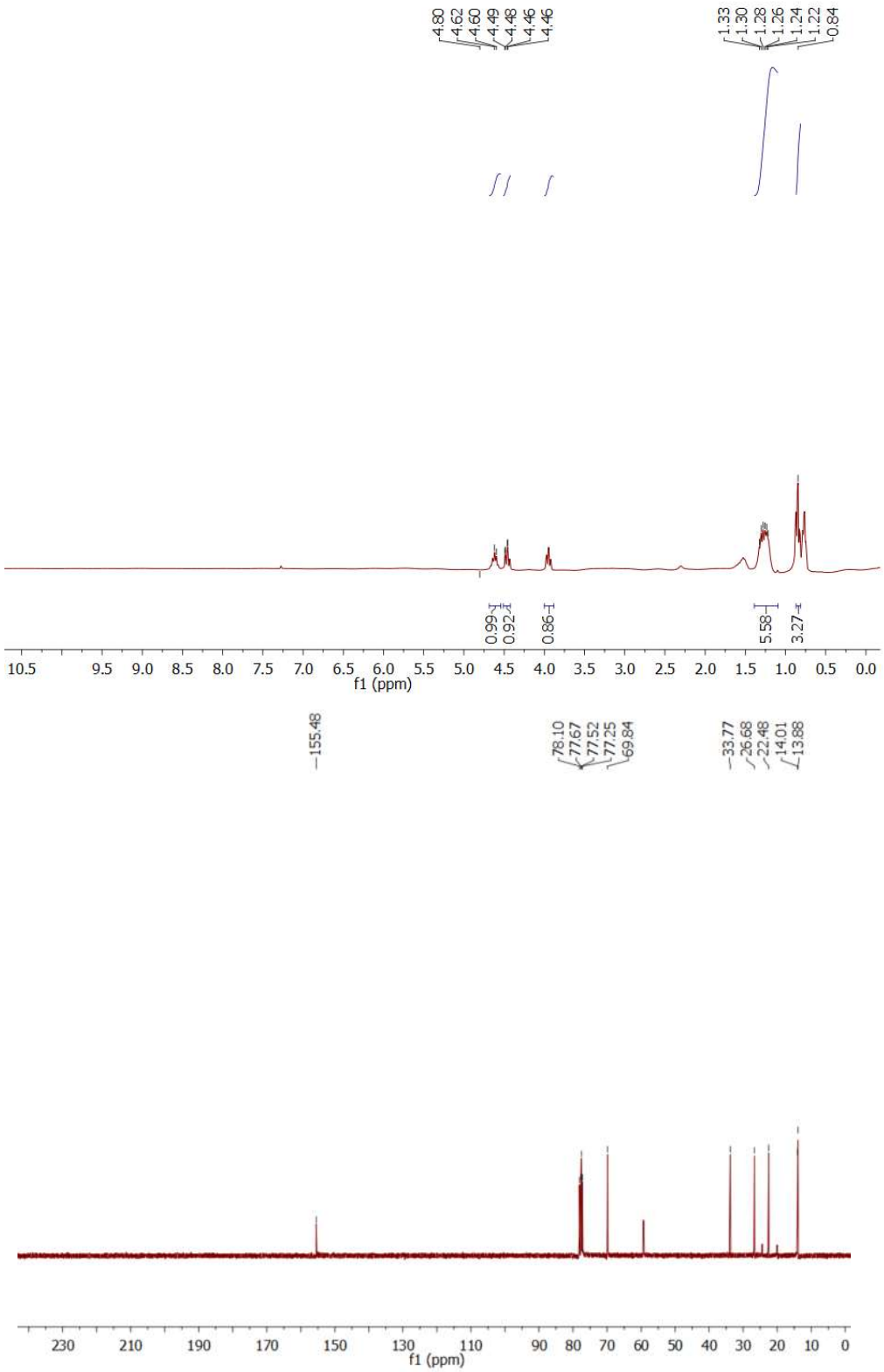

Figure S14. ^{1}H and ^{13}C NMR spectra of 4-butyl 1,3-dioxolan-2-one in $CDCl_3$.

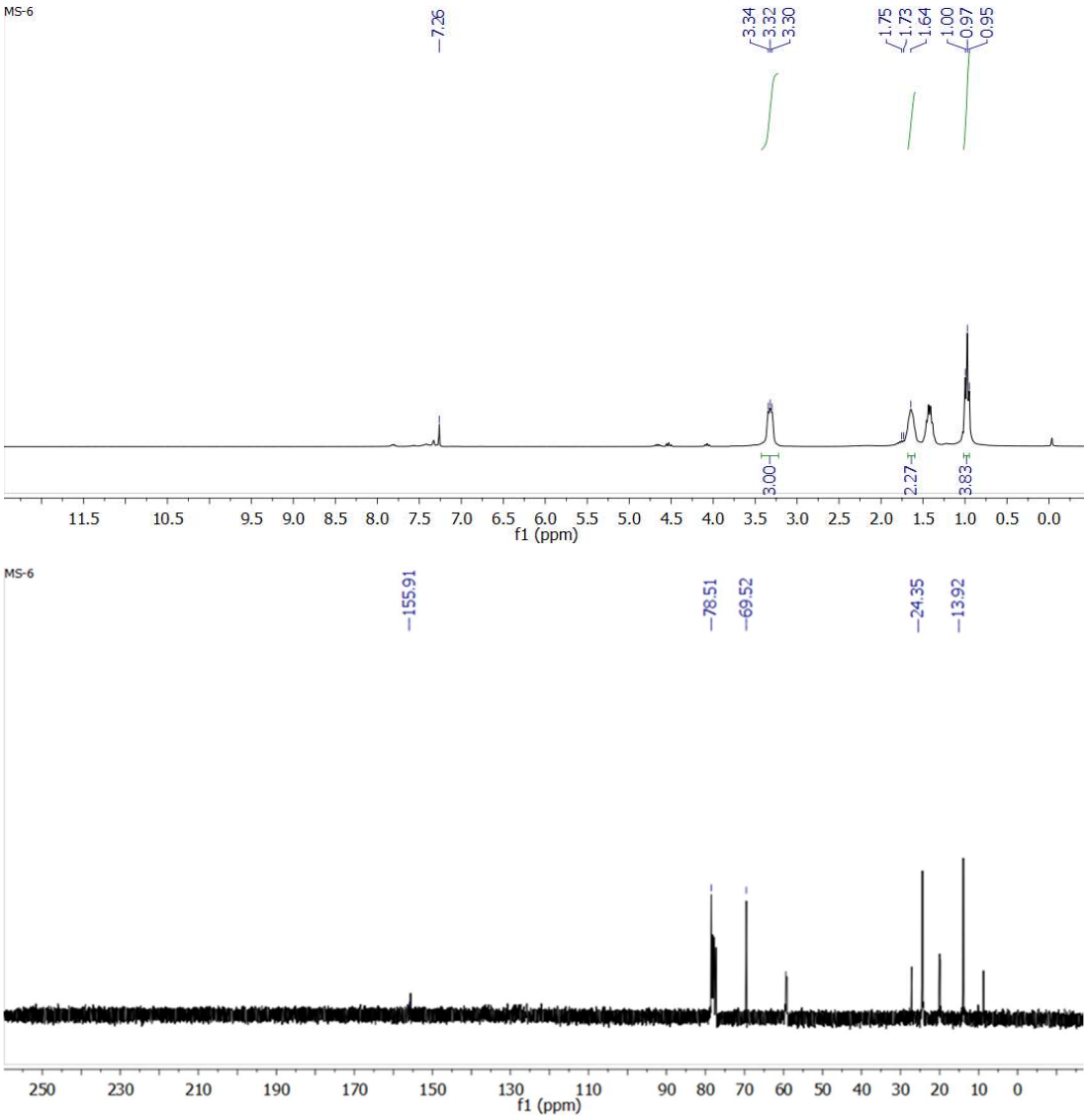

Figure S15. ^{1}H and ^{13}C NMR spectra of 4-ethyl-1,3-dioxolan-2-one.

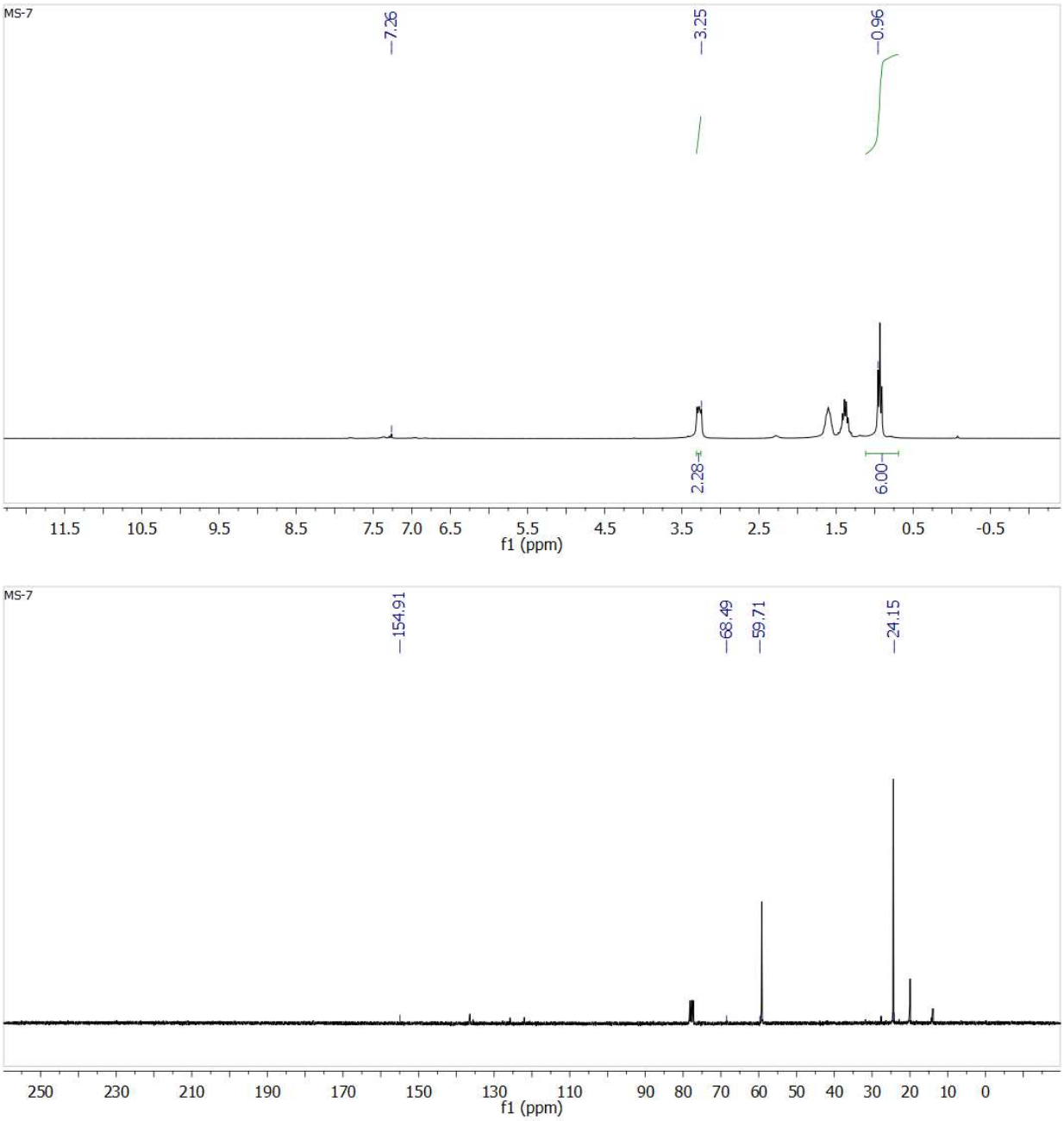

Figure S16. ^{1}H and ^{13}C NMR spectra of 4,4-dimethyl-1,3-dioxolan-2-one.

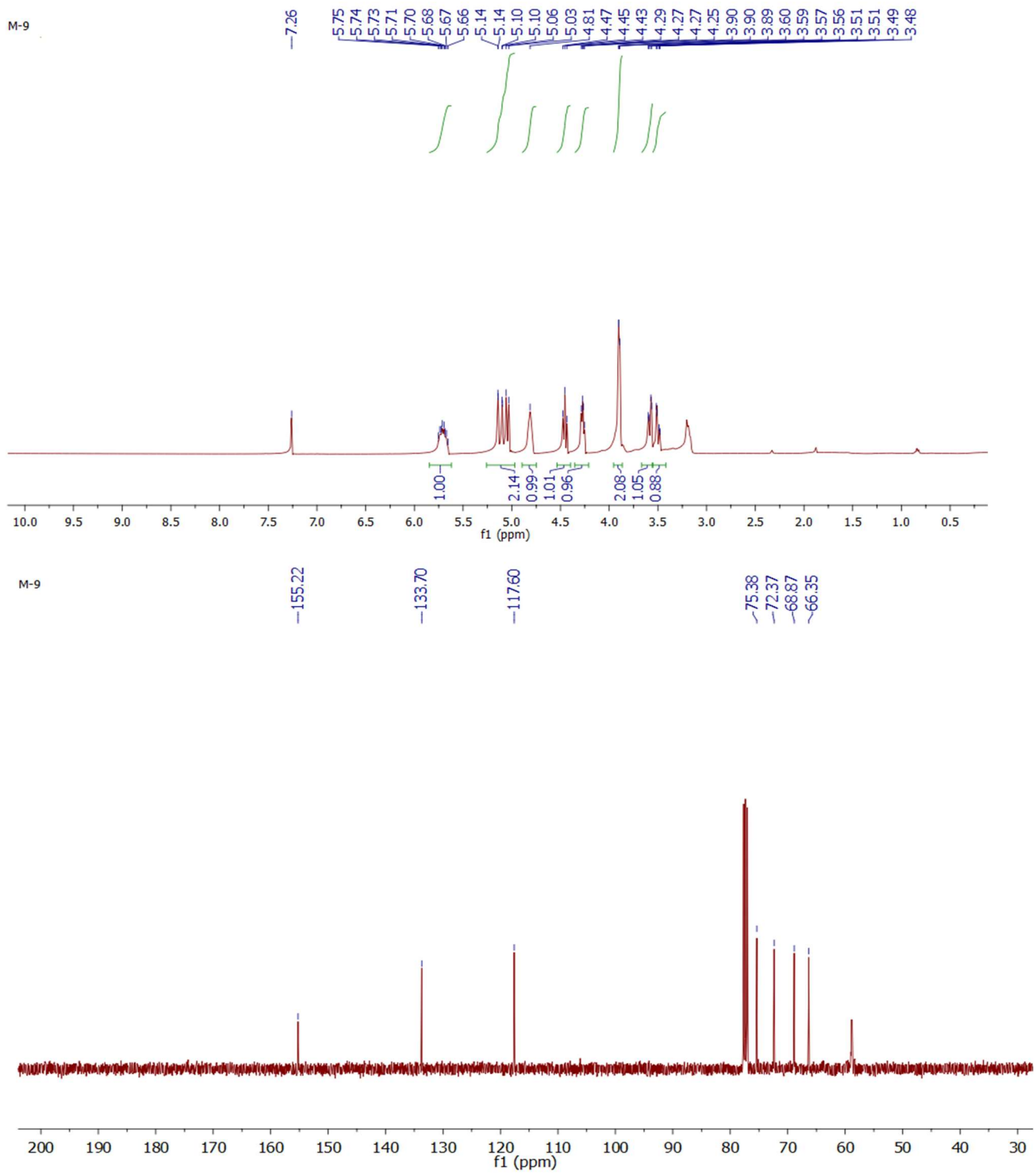

Figure S17. ^{1}H and ^{13}C NMR spectra of 4-(allyloxymethyl)-1,3-dioxolan-2-one.

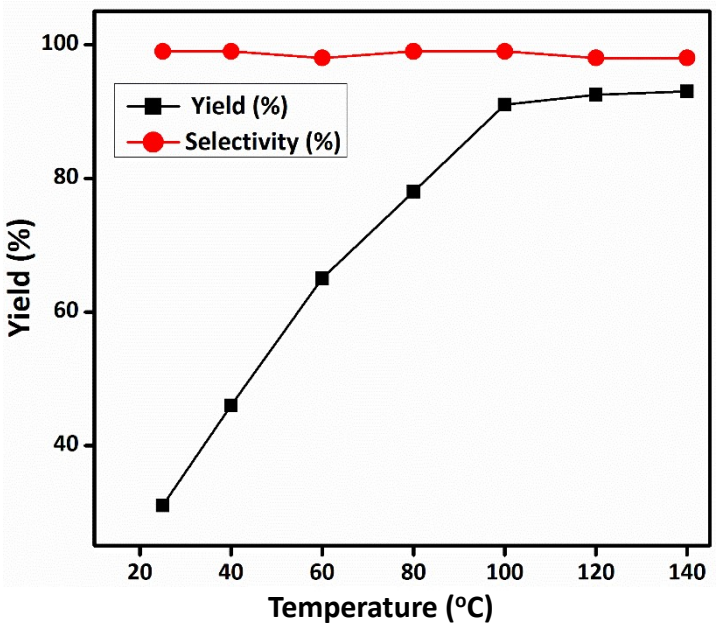

Figure S18. Temperature depended yield and selectivity of propylene carbonate production by **4** (2.5 μmol, 0.05 mol%), propylene oxide (5 mmol), Et_3N (5 μmol) under 1 atm CO_2 in CH_3CN (2 mL) for 8 hours with various temperature.

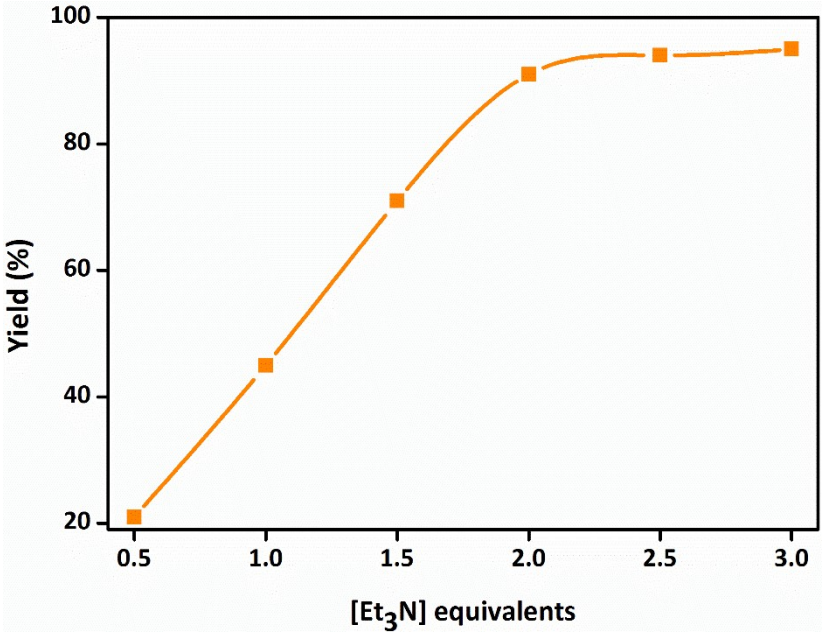

Figure S19. Influence of Et_3N for the CO_2 fixation reaction. Reaction condition: propyleneoxide (5 mmol), **4** (2.5 μmol, 0.05 mol%) and Et_3N (0.5 – 3 equivalents) in CH_3CN (2.0 mL) under 1 atm CO_2 at 100 °C over 8 hours.

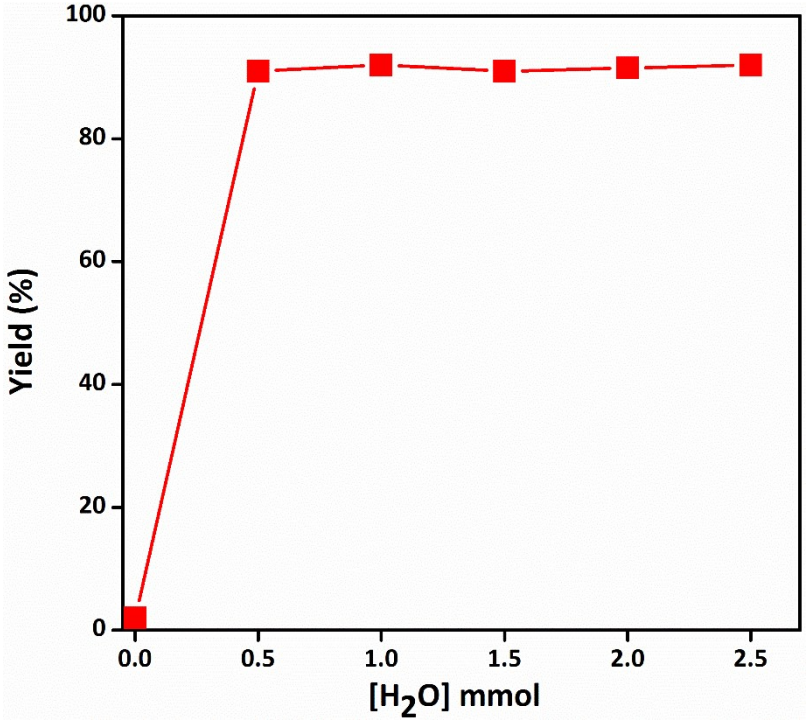

Figure S20. Influence of H_2O in the CO_2 fixation reaction. Reaction condition: propyleneoxide (5 mmol), **4** (2.5 μmol, 0.05 mol%) and Et_3N (5 μmol) in CH_3CN (2.0 mL), H_2O (0.5 – 2.5 mmol) under 1 atm CO_2 at 100 °C.

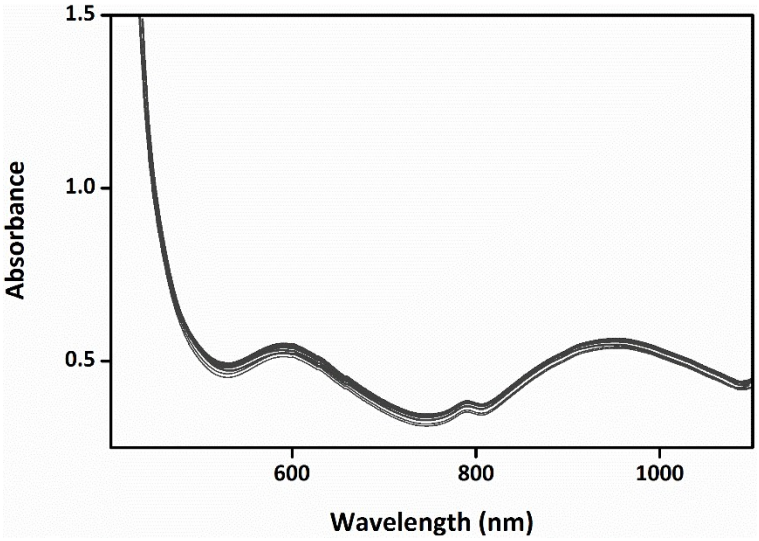

Figure S21. Electronic spectral change for the reaction of **4** (5×10^{-3} M) with O_2 and CO_2 in acetonitrile at 25 °C.

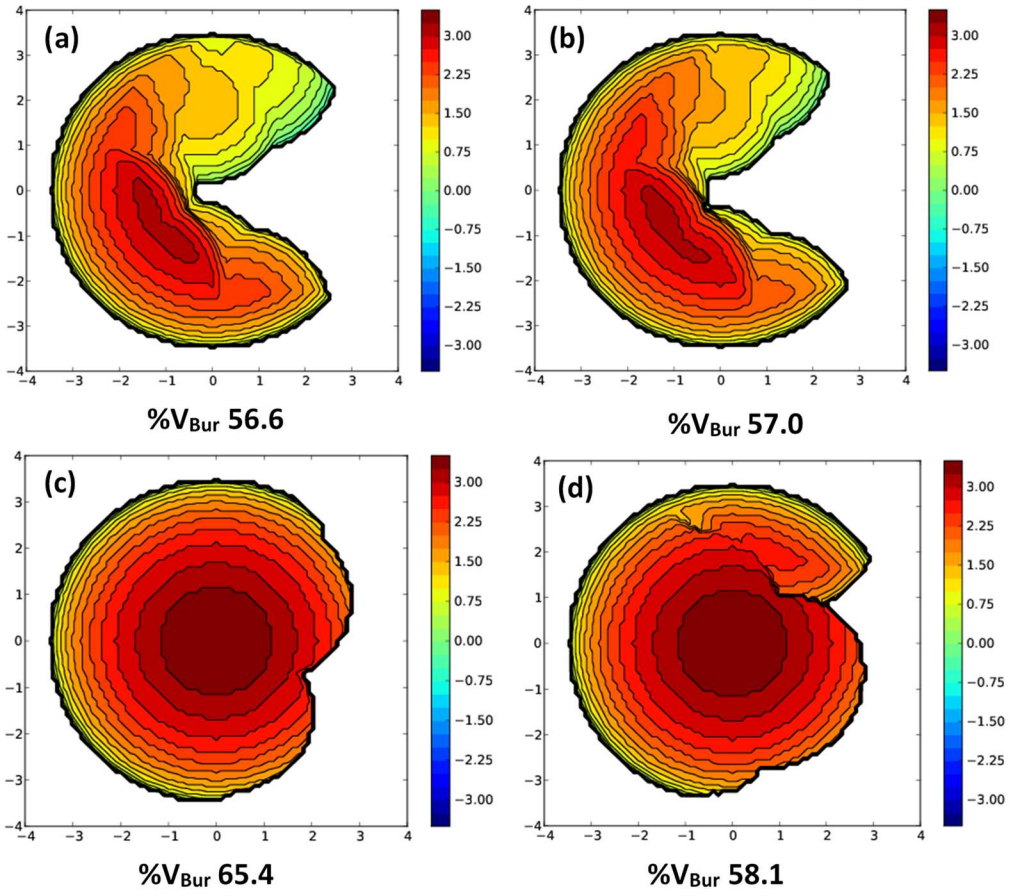

Figure S22. Steric map of complex **1 (a), 2 (b), 3 (c)** and **4 (d)** calculated by SambVca 2.1 A.

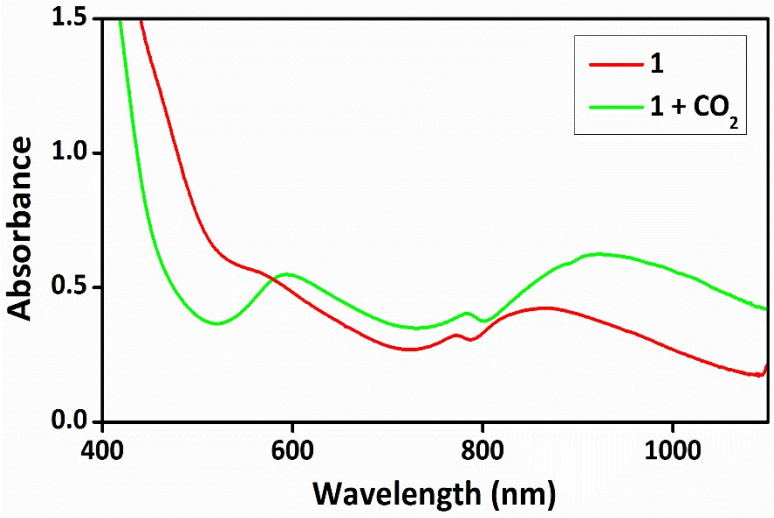

Figure S23. Electronic spectral change for the reaction of **1** (5×10^{-3} M) with CO_2 in acetonitrile at 25 °C.

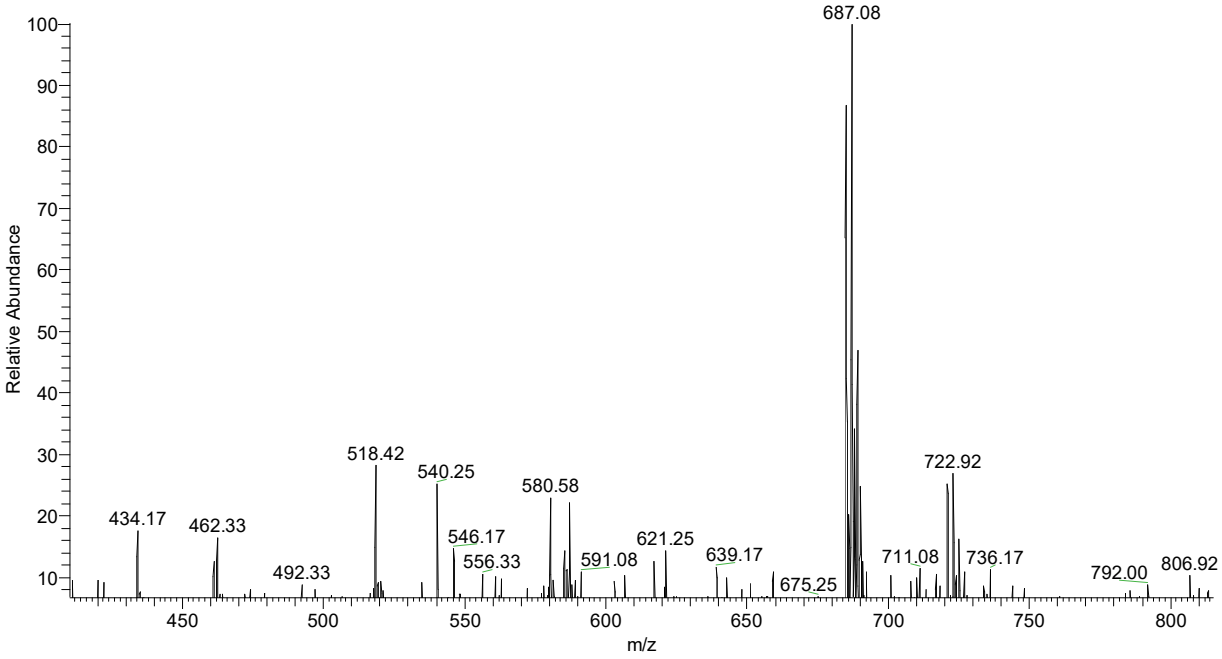

Figure S24. ESI-MS spectrum of **1a** in acetonitrile.

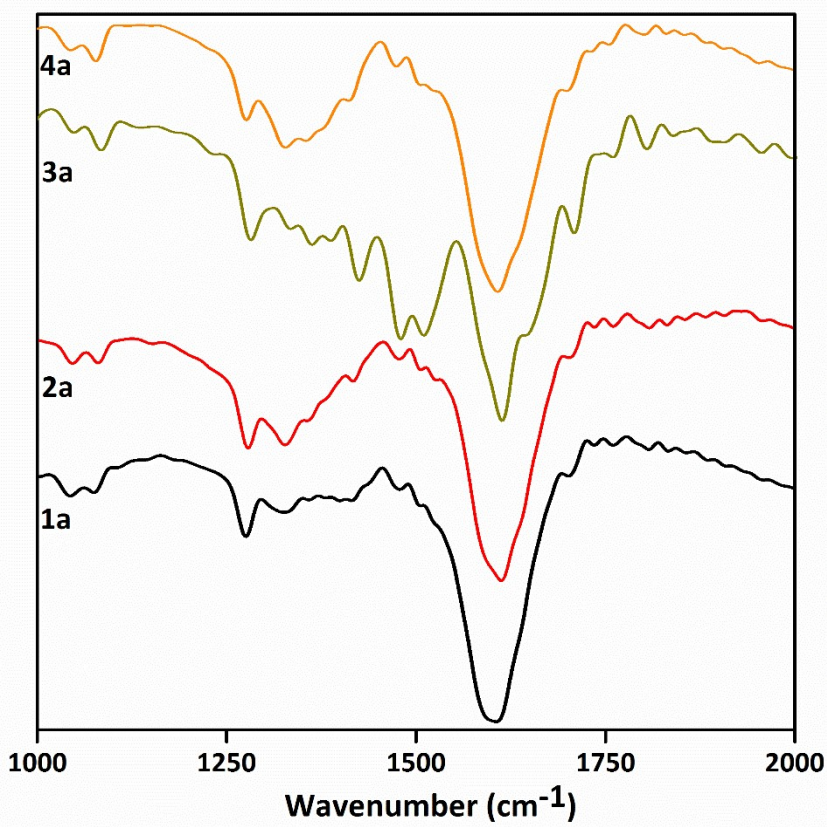

Figure S25. FT-IR spectra for **1a – 4a** using KBr.

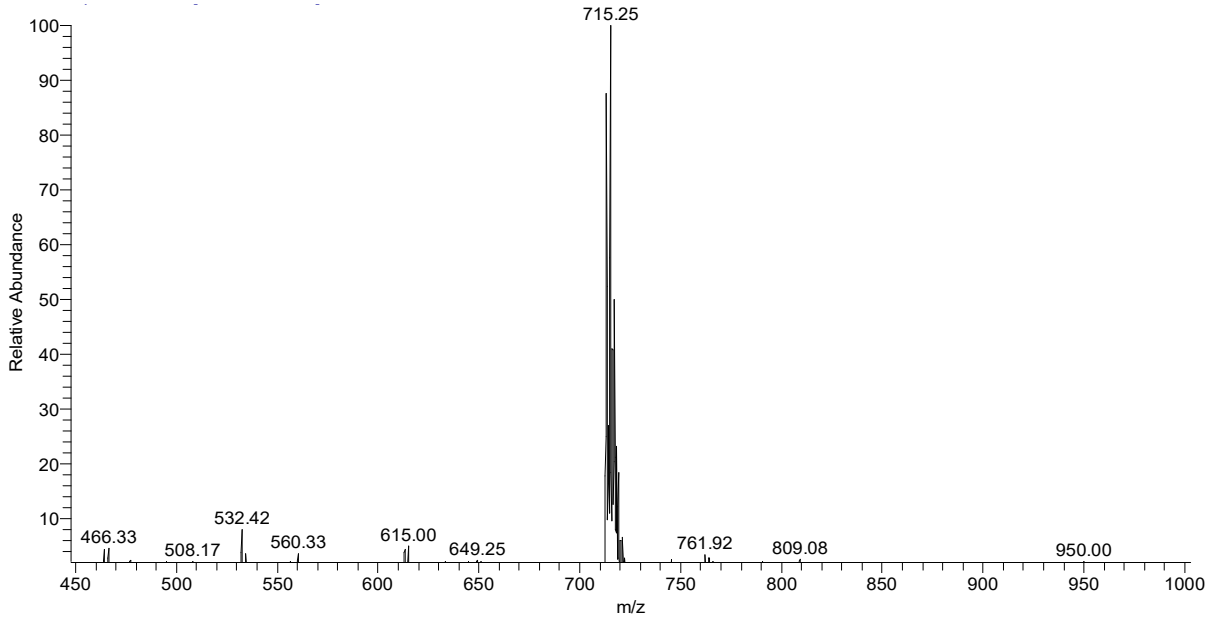

Figure S26. ESI-MS spectrum of **2a** in acetonitrile.

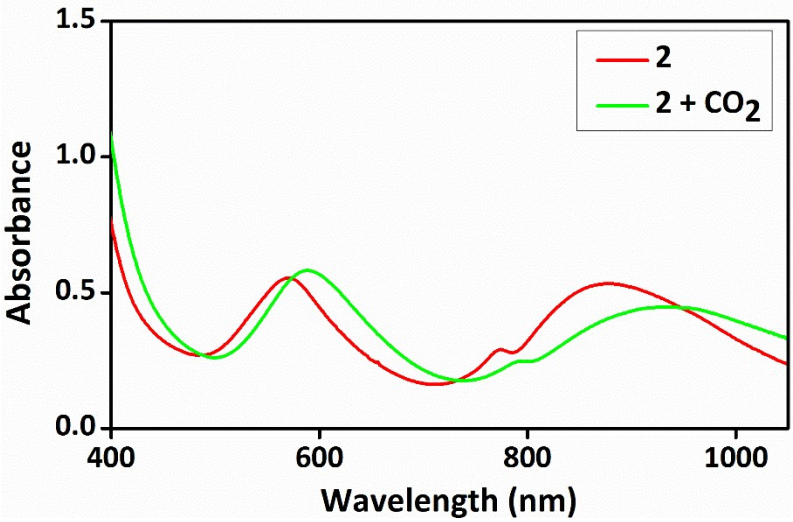

Figure S27. Electronic spectral change for the reaction of **2** (5×10^{-3} M) with CO_2 in acetonitrile at 25 °C.

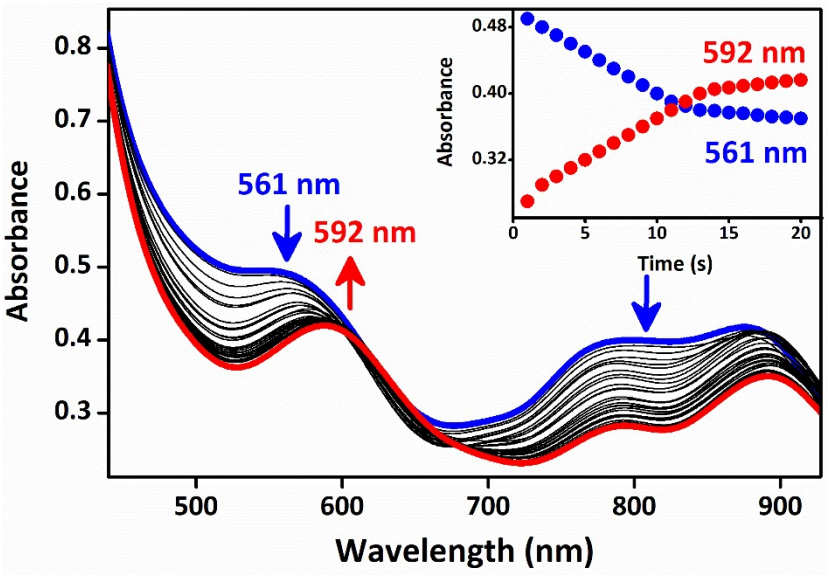

Figure S28. The kinetic behavior of the complex **2** (1×10^{-3} M) with CO_2 in the presence of two equivalent Et_3N in acetonitrile solution at 25 ˚C. The inset shows the time course of the absorbance at 561 and 592 nm.

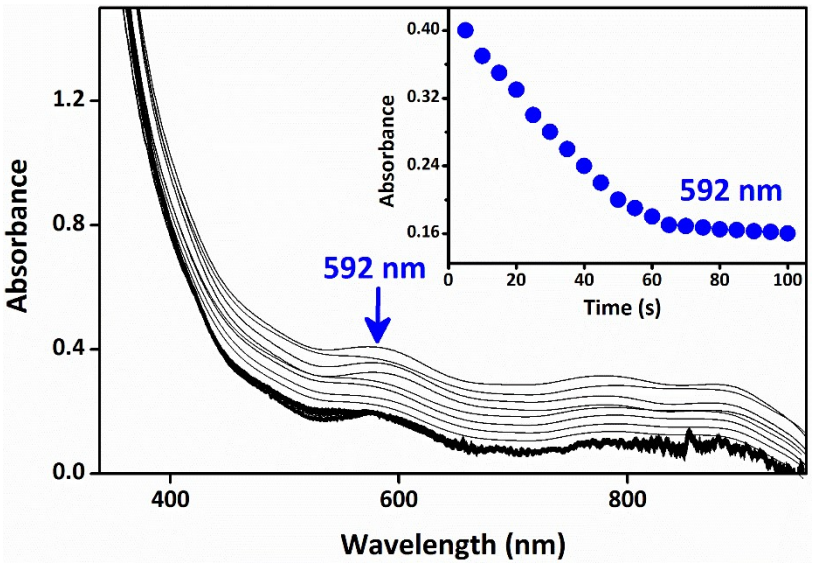

Figure S29. The reaction of $[(L2Ni)_2(CO_3)]^{2+}$ (1×10^{-3} M) with 50 equivalents of epichlorohydrin in acetonitrile at 70 °C. The inset shows the time course of the absorbance at 592 nm.

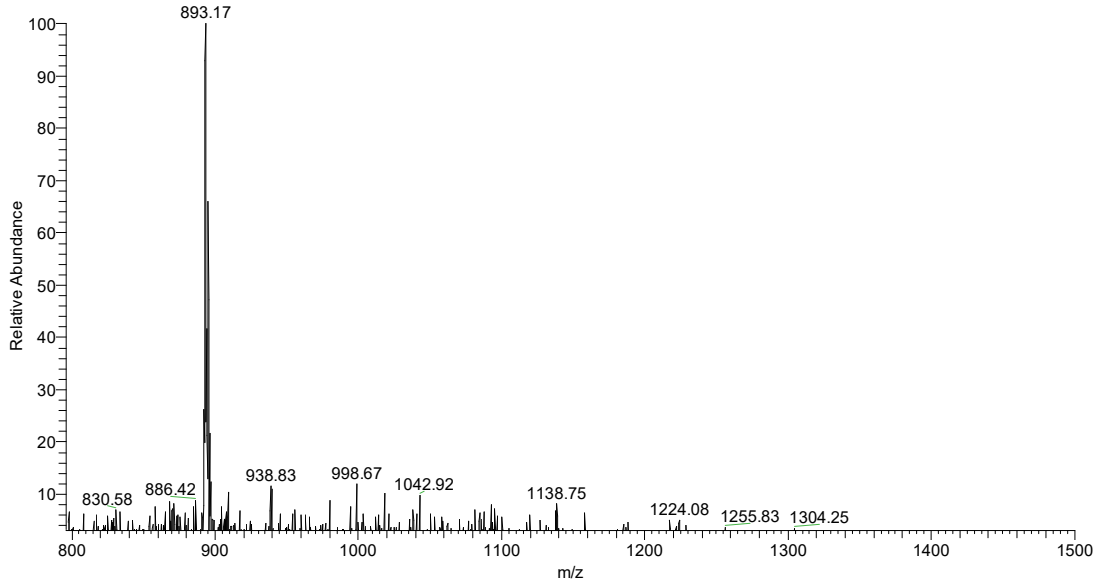

Figure S30. ESI-MS spectrum of **3a** in acetonitrile.

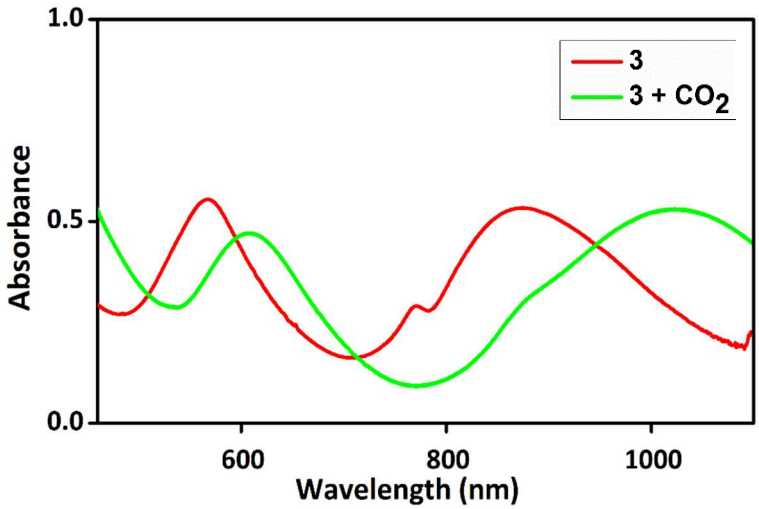

Figure S31. Electronic spectral change for the reaction of **3** (1×10^{-3} M) with CO_2 in acetonitrile at 25 °C.

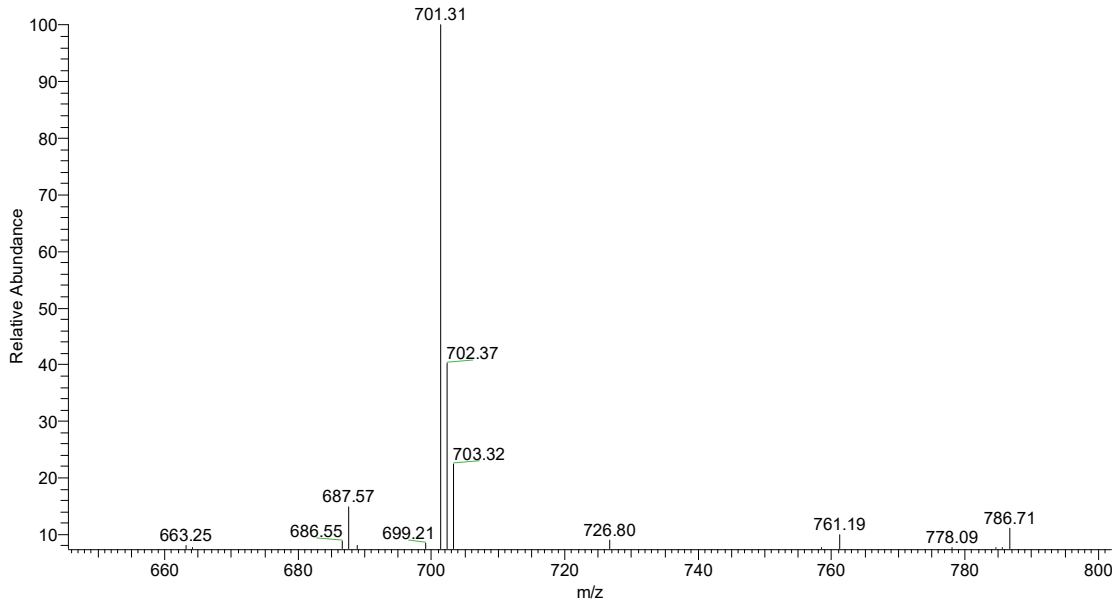

Figure S32. ESI-MS spectrum of **4a** in acetonitrile.

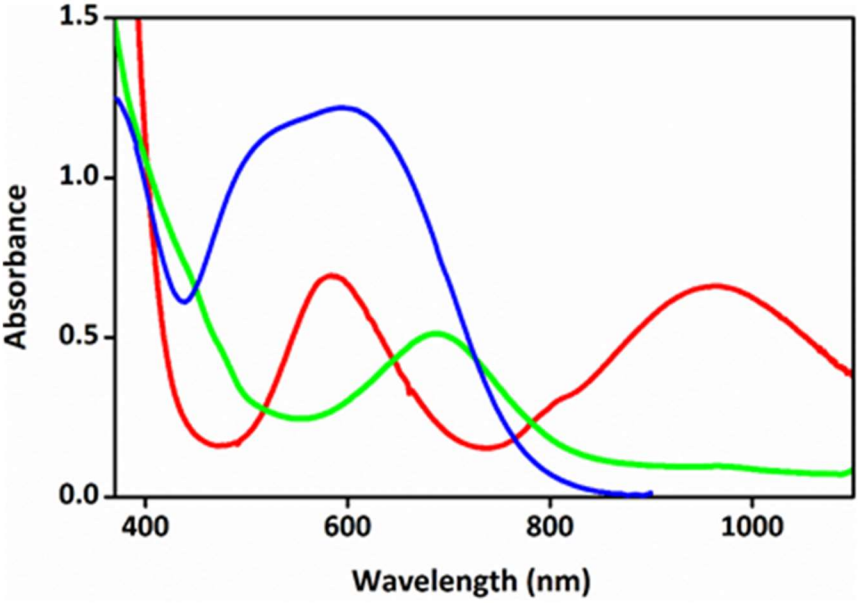

Figure S33. Absorption spectra of **4** (solid-state, blue), **4** (1×10^{-3} M) (red) and **4a** (1×10^{-3} M) in CH_3CN (green) at 25 °C.

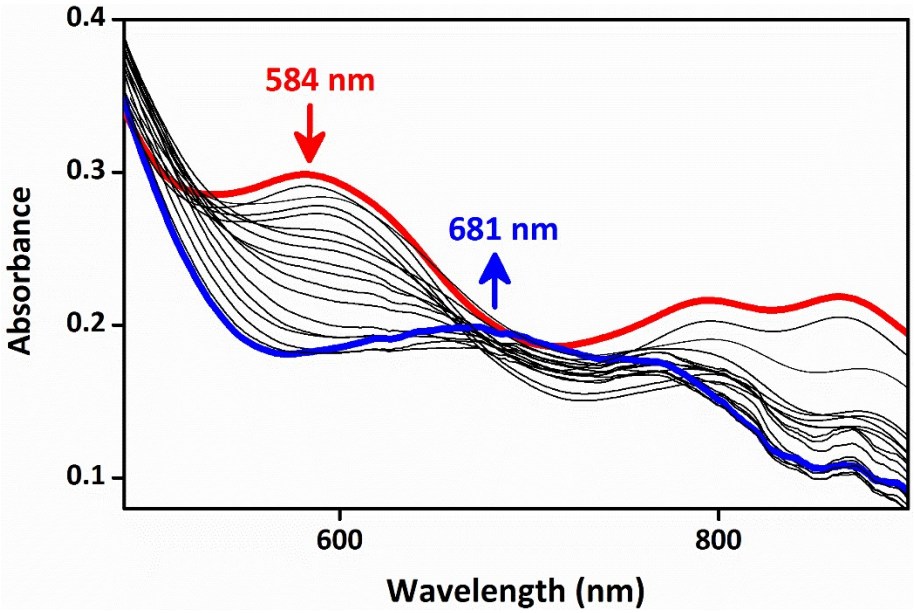

Figure S34. The kinetic behavior of the complex **4** (1×10^{-3} M) with CO_2 in the presence of two equivalent Et_3N in acetonitrile solution at 25 ˚C. The inset shows the time course of the absorbance at 584 and 581 nm.

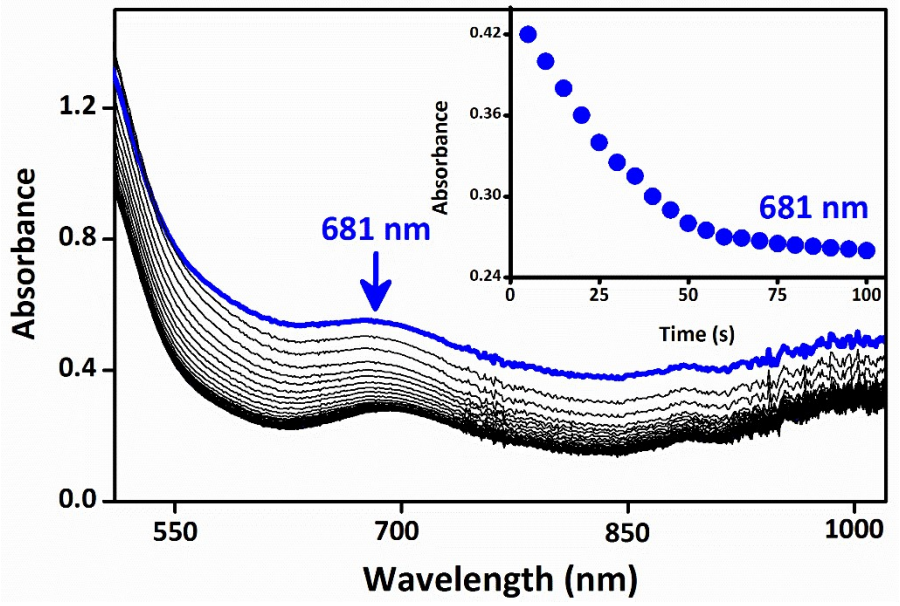

Figure S35. The reaction of $[(L4Ni)_2(CO_3)]^{2+}$ (1×10^{-3} M) with 50 equivalents of epichlorohydrin in acetonitrile at 70 °C. The inset shows the time course of the absorbance at 681 nm.

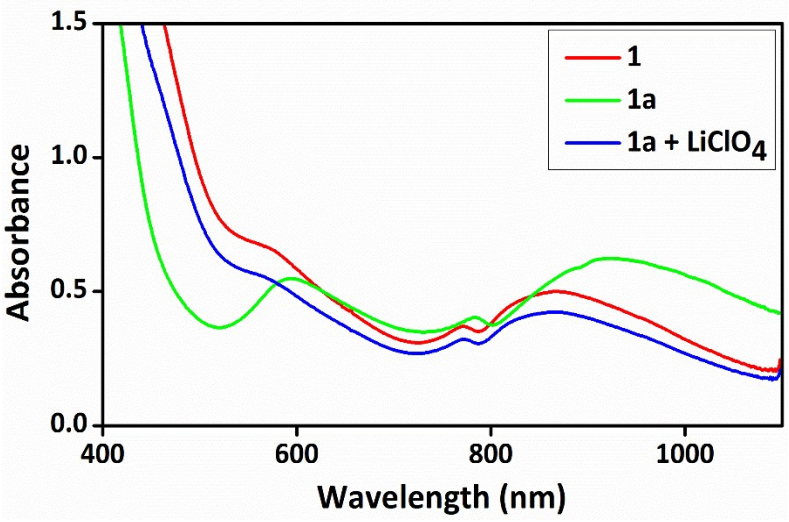

Figure S36. Electronic spectral change of complex **1**, **1a** and **1a** + $LiClO_4$ in acetonitrile at room temperature.

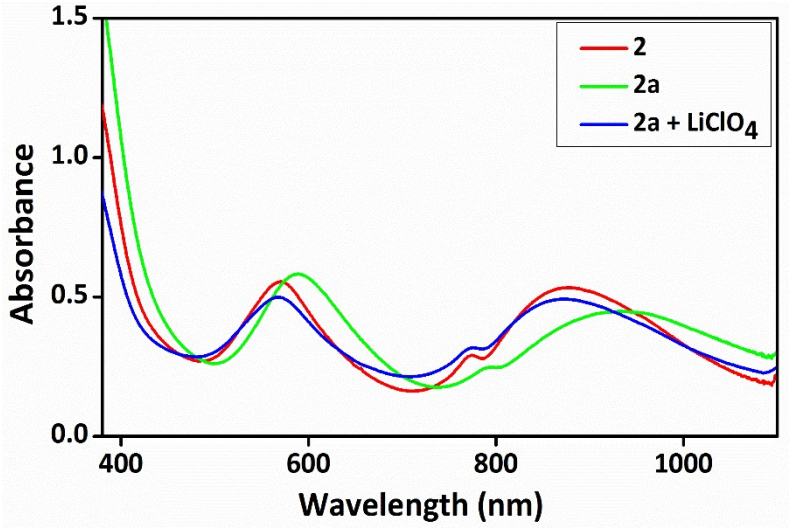

Figure S37. Electronic spectral change of complex **2, 2a** and **2a** + $LiClO_4$ in acetonitrile at room temperature.

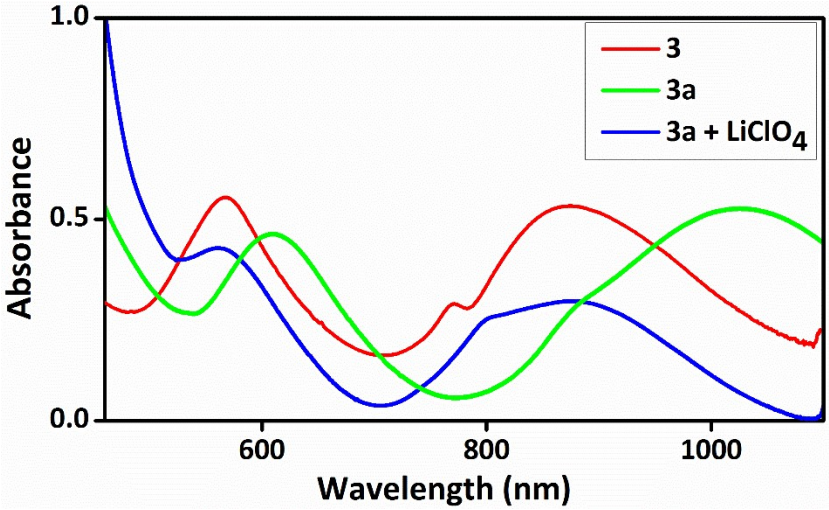

Figure S38. Electronic spectral change of complex **3**, **3a** and **3a** + $LiClO_4$ in acetonitrile at room temperature.

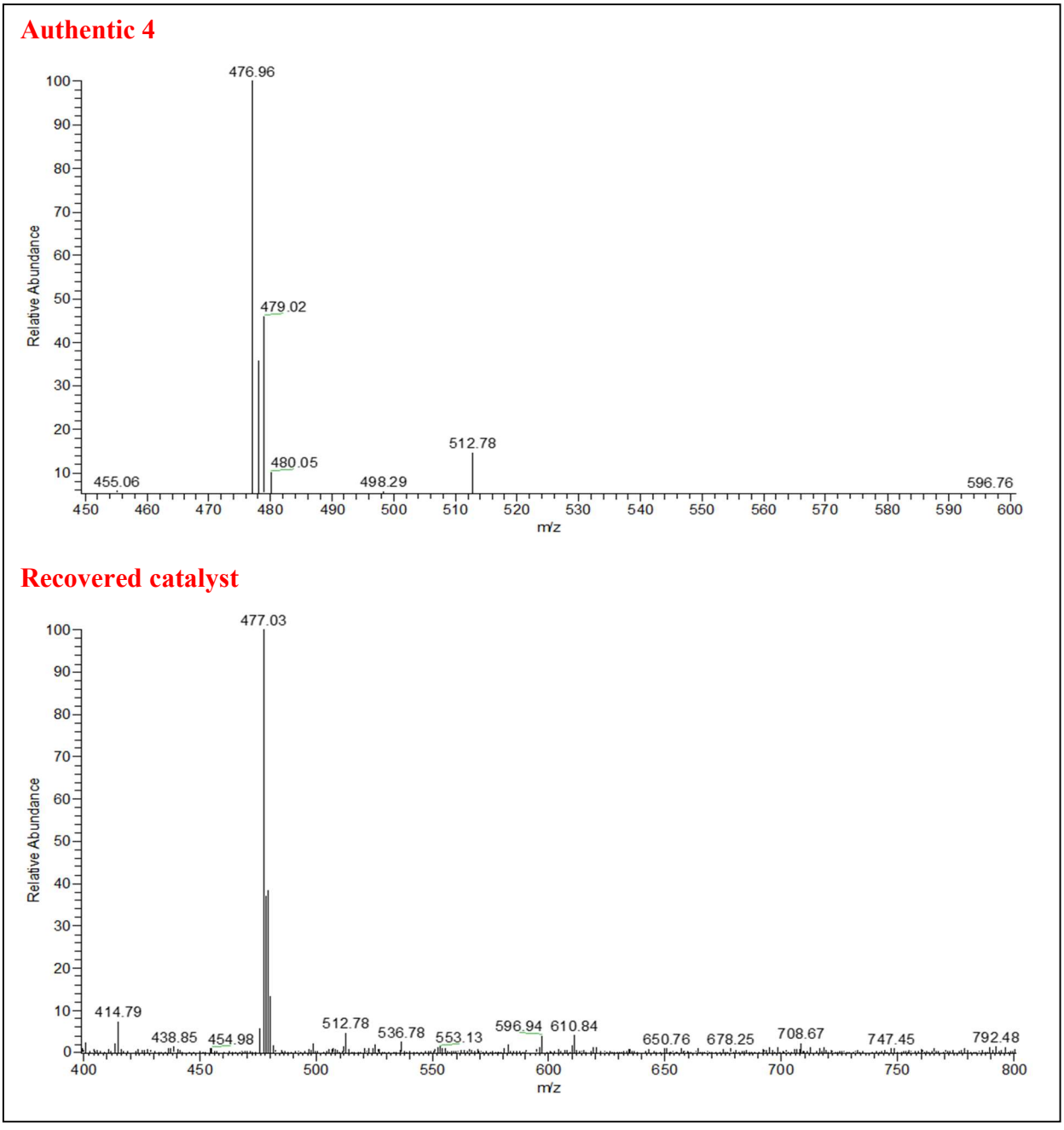

Figure S39. ESI-MS spectra of **4** (top) and regeneration of the catalyst **4** (bottom) in acetonitrile solution.

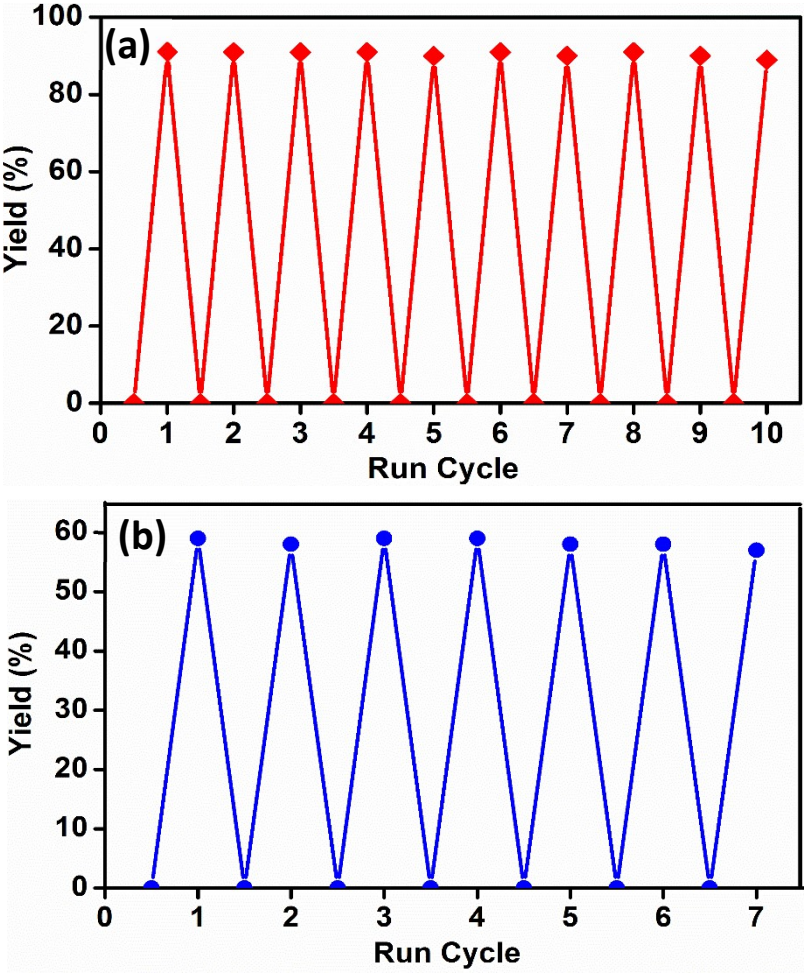

Figure S40. Recyclability test for **4** in the presence of CO_2 **(a)** and atmospheric air **(b)**.

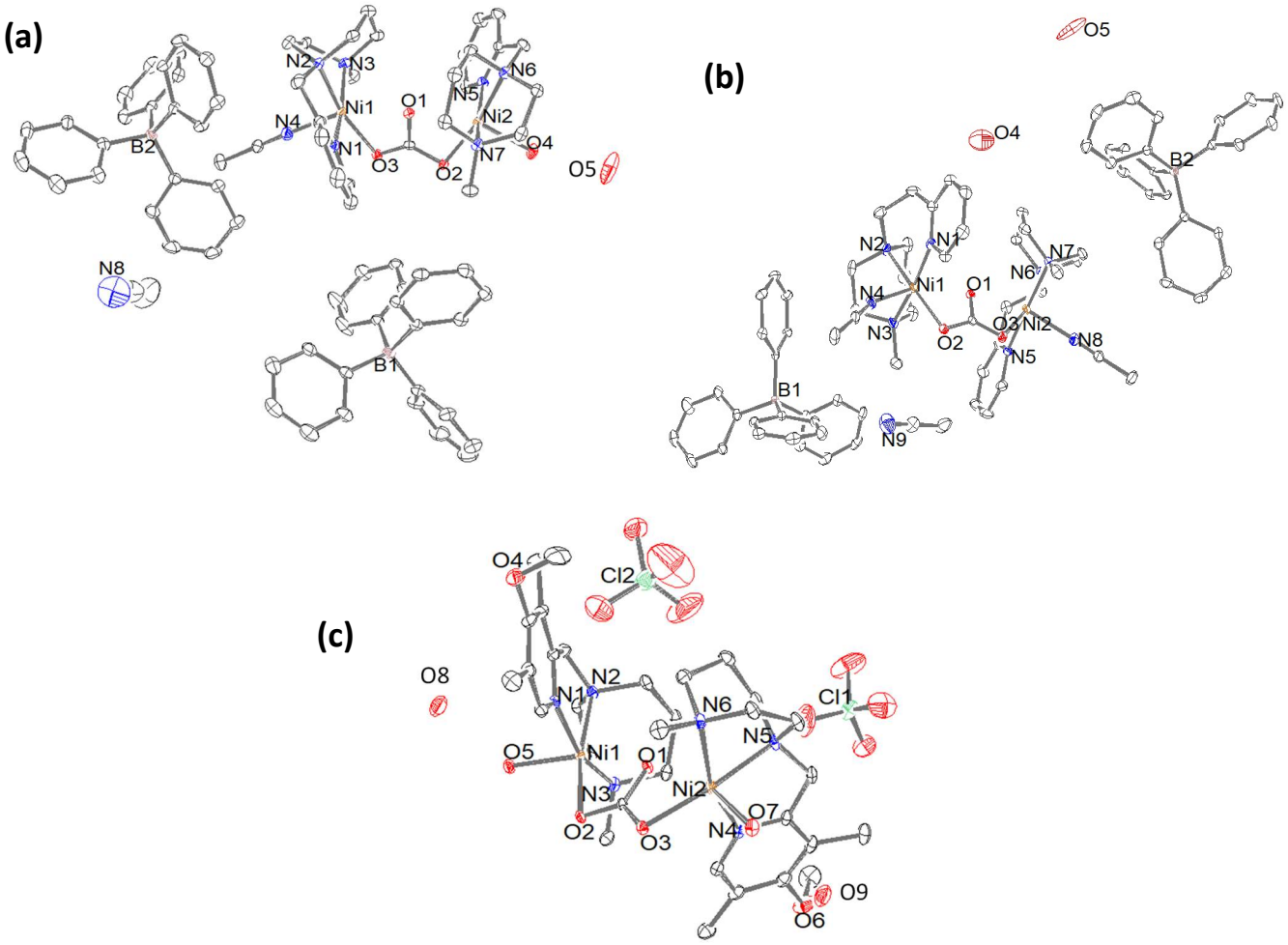

Figure S41. ORTEP plot for **1a (a), 2a (b)** and **4a (c)**. The probability ellipsoids are drawn at the 50% probability level. The H atoms are omitted for the clarity.

Table S1. Selected bond distances[a] (Å) bond angles[a] (°) of **1**

Bond lengths		Bond angles	
Ni(1)-N(1)	1.985(3)	N(1)-Ni(1)-N(3)	158.1(12)
Ni(1)-N(2)	2.152(3)	N(1)-Ni(1)-N(6)	93.8(12)
Ni(1)-N(3)	2.085(3)	N(1)-Ni(1)-N(2)	86.0(11)
Ni(1)-N(4)	2.175(3)	N(1)-Ni(1)-N(5)	95.1(13)
Ni(1)-N(5)	2.153(3)	N(1)-Ni(1)-N(4)	80.4(13)
Ni(1)-N(6)	2.120(3)	N(3)-Ni(1)-N(6)	88.42(13)
		N(3)-Ni(1)-N(2)	72.25(12)
		N(3)-Ni(1)-N(5)	106.73(12)
		N(3)-Ni(1)-N(4)	100.21(12)
		N(6)-Ni(1)-N(2)	88.27(13)
		N(6)-Ni(1)-N(5)	88.74(12)
		N(6)-Ni(1)-N(4)	169.13(13)
		N(2)-Ni(1)-N(4)	100.51(12)
		N(5)-Ni(1)-N(4)	82.6(13)

[a]Standard deviations in parenthesis

Table S2. Calculated bond distance and bond angle for **2 - 4** by DFT method

	2	**3**	**4**
Bond length			
Ni(1)-N(1)	2.139	2.125	2.061
Ni(1)-N(2)	2.204	2.208	2.132
Ni(1)-N(3)	2.143	2.150	2.148
Ni(1)-N(4)	2.130	2.136	2.123
Ni(1)-N(5)	2.066	2.137	2.161
Ni(1)-N(6)	2.351	2.252	2.141
Bond Angle			
N(1)-Ni(1)-N(3)	160.63	156.58	159.07
N(1)-Ni(1)-N(6)	94.56	83.54	86.17
N(1)-Ni(1)-N(2)	83.48	81.02	82.24
N(1)-Ni(1)-N(5)	84.46	91.45	100.60
N(1)-Ni(1)-N(4)	85.64	83.26	88.98
N(3)-Ni(1)-N(6)	98.57	91.84	95.68
N(3)-Ni(1)-N(2)	76.40	74.65	76.98
N(3)-Ni(1)-N(5)	115.54	105.82	93.79
N(3)-Ni(1)-N(4)	79.121	85.69	100.31
N(6)-Ni(1)-N(2)	103.33	79.65	102.08
N(6)-Ni(1)-N(5)	163.45	157.81	165.28
N(6)-Ni(1)-N(4)	75.14	86.32	83.365
N(2)-Ni(1)-N(4)	167.33	172.32	174.069
N(5)-Ni(1)-N(4)	81.22	80.35	83.88

Table S3. The electronic spectral, redox data of the nickel(II) complexes and their CO_2 adducts

Complex	Electronic Spectra[a]	Redox data[c]				
		Ep_a	Ep_c	ΔE (mV)	$E_{1/2}$ (V)	
	λ_{max}, nm, (ε, M^{-1} cm^{-1})	(V)	(V)		CV	DPV
1	542 (351), 769 (270), 845 (348). 610[b]	-0.515	-0.771	256	-0.643	-0.621
1a	596 (273), 794 (183), 896 (291)	-0.590	-0.831	241	-0.710	
2	561 (491), 776 (390), 883 (417). 640[b]	-0.551	-0.820	269	-0.685	-0.646
2a	592 (501), 794 (247), 927 (447)	-0.643	-0.869	226	-0.756	
3	569 (554), 770 (290), 874 (533). 520[b]	-0.432	-0.663	231	-0.547	-0.592
3a	608 (520), 800 (308), 1010 (560)	-0.605	-0.820	215	-0.712	
4	584 (291), 791 (210), 864 (218). 580[b]	-0.614	-0.793	190	-0.703	-0.691
4a	681 (205), 794 (156), 872 (120)	-0.669	-0.879	210	-0.774	

[a]Concentration: 1×10^{-3} M in acetonitrile. [b]In diffuse reflectance. [c]Concentration: 1×10^{-3} M in acetonitrile; supporting electrolyte: 0.1 M TBAP. Working electrode: Pt sphere, reference electrode: Ag/Ag^{+} and counter electrode: Pt wire.

Table S4. Optimization of the reaction of propylene oxide with 1 atm CO_2 using **4**

Entry[a]	Catalyst (mol%)	Temperature (°C)	Yield[d] (%)	TON	TOF (h^{-1})	Selectivity (%)
1	0.025	25	16	320	40	>99
2	0.05	25	31	620	78	>99
3	0.05	40	42	840	105	>99
4	0.05	60	65	1300	163	>99
5	0.05	80	78	1560	195	>99
6	0.05	100	91	1820	228	>99
7	0.05	120	93	1860	233	>99
8	-	100	4	80	10	>99
9[b]	0.05	100	6	120	15	-
10[c]	0.05	100	78	1560	195	>99
11[d]	0.05	100	82	1640	205	>99
12[e]	0.05	100	64	1280	160	>99

[a]Propylene oxide (5 mmol). [b]Absence of Et_3N. [c]using catalyst **1**. [d]using catalyst **2**. [e]using catalyst **3**.

Table S5. Selected bond distances[a] (Å) bond angles[a] (°) for **1a** and **2a**.

$[(L1Ni)_2(\mu\text{-}CO_3)(H_2O)(CH_3CN)](CH_3CN)(BPh_4)_2$ **1a**

Bond Distance

Ni(1)-N(1)	2.056	Ni(2)-N(6)	2.067	Ni(1)-N(2)	2.072
Ni(2)-N(7)	2.099	Ni(1)-N(3)	2.099	Ni(1)-O(1)	2.057
Ni(1)-N(4)	2.075	Ni(2)-O(2)	2.044	Ni(2)-N(5)	2.071
Ni(2)-O(4)	2.100				

Bond Angle

N(1)-Ni(1)-N(3)	160.6	O(4)-Ni(2)-O(2)	93.5	N(1)-Ni(1)-N(4)	92.8
N(5)-Ni(2)-O(4)	93.1	N(1)-Ni(1)-N(2)	83.1	N(7)-Ni(2)-O(4)	93.5
N(1)-Ni(1)-O(3)	95.7	N(6)-Ni(2)-O(2)	170.0	N(2)-Ni(1)-O(3)	165.8
N(5)-Ni(2)-O(2)	94.2	N(3)-Ni(1)-O(3)	101.7	N(7)-Ni(2)-O(2)	103.8
N(4)-Ni(1)-O(3)	96.0	N(6)-Ni(2)-N(5)	83.1	N(2)-Ni(1)-N(3)	77.8
N(6)-Ni(2)-N(7)	77.7	N(4)-Ni(1)-N(3)	93.5	N(5)-Ni(2)-N(7)	160.2
N(6)-Ni(2)-O(4)	96.1				

$[(L2Ni)_2(\mu\text{-}CO_3)(CH_3CN)_2](BPh_4)_2(CH_3CN)_2$ **2a**

Bond Distance

Ni(1)-N(1)	2.146(3)	Ni(2)-N(5)	2.138(4)	Ni(2)-N(8)	2.077(4)
Ni(1)-N(2)	2.066(3)	Ni(2)-N(6)	2.075(3)	Ni(1)-O(1)	2.041(3)
Ni(1)-N(3)	2.105(3)	Ni(2)-N(7)	2.127(3)	Ni(2)-O(2)	2.029(3)
Ni(1)-N(4)	2.088(4)				

Bond Angle

N(2)-Ni(1)-O(1)	165.60(13)	N(6)-Ni(2)-O(2)	170.62(13)
N(4)-Ni(1)-O(1)	95.80(14)	N(8)-Ni(2)-O(2)	89.02(13)
N(4)-Ni(1)-N(2)	97.37(15)	N(6)-Ni(2)-N(8)	98.17(15)
N(3)-Ni(1)-O(1)	91.38(13)	N(7)-Ni(2)-O(2)	92.17(12)
N(2)-Ni(1)-N(3)	94.70(14)	N(6)-Ni(2)-N(7)	93.71(14)
N(4)-Ni(1)-N(3)	88.82(15)	N(7)-Ni(2)-N(8)	90.95(15)
N(1)-Ni(1)-O(1)	97.08(13)	N(5)-Ni(2)-O(2)	97.57(13)
N(1)-Ni(1)-N(2)	77.01(14)	N(5)-Ni(2)-N(6)	76.21(15)
N(1)-Ni(1)-N(4)	90.57(15)	N(8)-Ni(1)-N(5)	92.42(15)
N(1)-Ni(1)-N(3)	171.54(14)	N(7)-Ni(2)-N(5)	169.74(14)

[a]Standard deviations in parenthesis

Table S6. Selected bond distances[a] (Å) bond angles[a] (°) for **4a**.

$[(L4Ni)_2(\mu\text{-}CO_3)(H_2O)_2(C_3H_6O)](ClO_4)_2$ **4a**					
Bond Distance					
Ni(1)-N(1)	2.055(5)	Ni(2)-N(5)	2.075(5)	Ni(2)-O(6)	2.221(4)
Ni(1)-N(2)	2.070(5)	Ni(2)-N(6)	2.112(6)	Ni(1)-O(1)	2.054(4)
Ni(1)-N(3)	2.096(5)	Ni(2)-N(4)	2.052(4)	Ni(2)-O(2)	2.064(4)
Ni(1)-O(4)	2.249(4)				
Bond Angle					
N(1)-Ni(1)-N(2)	81.9(2)		O(6)-Ni(2)-N(4)	94.0(2)	
O(1)-Ni(1)-N(1)	96.88(2)		O(2)-Ni(2)-N(4)	95.42(19)	
O(1)-Ni(1)-N(2)	168.58(5)		O(6)-Ni(2)-O(2)	97.33(17)	
O(1)-Ni(1)-O(4)	97.66(17)		N(4)-Ni(2)-N(5)	82.7(2)	
N(1)-Ni(1)-O(4)	93.2(2)		O(6)-Ni(2)-N(5)	171.08(17)	
N(2)-Ni(1)-O(4)	93.74(19)		N(4)-Ni(2)-N(6)	159.4(2)	
O(1)-Ni(1)-N(3)	101.8(2)		N(4)-Ni(2)-N(6)	91.7(2)	
N(3)-Ni(1)-N(1)	159.6(2)		O(2)-Ni(2)-N(6)	103.44(19)	
N(2)-Ni(1)-N(3)	78.2(2)		N(5)-Ni(2)-N(6)	74.4(2)	
N(3)-Ni(1)-O(4)	92.34(19)		N(4)-Ni(2)-O(2)	87.63(5)	

Table S7. Crystal data and structure refinement for complexes **1, 1a, 2a** and **4a**.

	1	**1a**	**2a**	**4a**
Formula	$NiC_{67}H_{68}B_2N_6$	$Ni_2C_{77}H_{86}B_2N_8O4$	$Ni_2C_{83}H_{94}B_2N_{10}O_3$	$Ni_2C_{34}H_{64}Cl_2N_6O_{18}$
Fw	1044.60	1326.57	1418.72	1033.23
Crystal system	Monoclinic	Triclinic	Orthorhombic	Orthorhombic
Space group	P 21/c	P-1	P n a21	P 21 21 21
Temperature	293(2) K	291(2) K	291(2) K	291(4) K
a/Å	24.8742(10)	13.9721(5)	31.3574(16)	11.7462(7)
b/Å	17.6602(8)	14.2148(5)	11.0783(5)	15.1861(9)
c/A^0	26.6397(11)	20.9208(10)	21.4842(10)	25.9560(16)
$\alpha/^0$	90	92.908(3)	90	90
$\beta/^0$	96.624(4)	106.598(3)	90	90
$\gamma/^0$	90	113.393(3)	90	90
Volume/$Å^3$	11624.3(9)	3590.5(3)	7463.3(6)	4630.0(5)
Z	4	2	4	4
ρ_{calc} mg/mm^3	1.196	1.227	1.263	1.482
μ/mm^{-1}	0.380	0.578	0.561	1.005
F(000)	4440	1404.0	3008.0	2176
Reflection collected	26525	14089	12818	12549
Goodness-of-fit on F^2	1.020	1.023	1.038	1.022
R1[a]	0.0942	0.0494	0.0396	0.0552
wR2[b]	0.2901	0.1228	0.0708	0.1285

s

$R1=\sum ||F_o|-|Fc||/\sum |F_o|$ $WR_2=\sum w[(F_o-F_c)^2/\sum w[(F_o^2)^2]^{1/2}$

Reply for A and B-level Check CIF alerts

Complex 1

PLAT330_ALERT_2_A Large Aver Phenyl C-C Dist C105--C110. 1.43 Ang.
PLAT330_ALERT_2_A Large Aver Phenyl C-C Dist C117--C122. 1.43 Ang.
PLAT331_ALERT_2_A Small Aver Phenyl C-C Dist C57--C62. 1.34 Ang.
PLAT331_ALERT_2_A Small Aver Phenyl C-C Dist C69--C74. 1.35 Ang.
PLAT331_ALERT_2_A Small Aver Phenyl C-C Dist C111--C116. 1.34 Ang.
PLAT330_ALERT_2_B Large Aver Phenyl C-C Dist C75--C80. 1.43 Ang.
PLAT330_ALERT_2_B Large Aver Phenyl C-C Dist C81--C86. 1.42 Ang.
PLAT331_ALERT_2_B Small Aver Phenyl C-C Dist C63--C68. 1.36 Ang.
PLAT331_ALERT_2_B Small Aver Phenyl C-C Dist C87--C92. 1.35 Ang.
PLAT331_ALERT_2_B Small Aver Phenyl C-C Dist C93--C98. 1.35 Ang.

Author Response: These alerts are generated by the possible disorder or substantial thermal mobility of the tetraphenylamines.

PLAT213_ALERT_2_B Atom C30 has ADP max/min Ratio..... 4.6 prolat

Author Response: These alerts are generated because there is a large amount of disorder in the structure.

PLAT410_ALERT_2_B Short Intra H...H Contact H24A..H27B. 1.82 Ang.
x,y,z = 1_555 Check

Author Response: The crystal was weakly diffracting and thus the quality of data is \ relatively poor. For that, the hydrogen atoms were included in geometrically calculated position and were refined according to the riding model.

PLAT910_ALERT_3_B Missing # of FCF Reflection(s) Below Theta (Min). 45 Note

Author Response: The unit cell is reasonable large and these low angle reflections are probably missing due to the beamstop.

Complex-1a

PLAT420_ALERT_2_B D-H Without Acceptor O22 --H22C. Please Check

Author Response: The bond O4-H40 is directed to a cavity whose disordered atomic content has been removed by SQUEEZE.